**Abstract** Photoconductive antennas are promising sources of terahertz radiation that is widely used for spectroscopy, characterization, and imaging of biological objects, deep space studies, scanning of surfaces, and detection of potentially hazardous substances. These antennas are compact and allow for generation of both ultrabroadband pulses and tunable continuous wave terahertz signals at room temperatures, with no need for high-power optical sources. However, such antennas have relatively low energy conversion efficiency of femtosecond laser pulses or two close pump wavelengths (photomixers) into the pulsed and continuous terahertz radiation, correspondingly. Recently, an approach to solving this problem that involves known methods of nanophotonics applied to terahertz photoconductive antennas and photomixers has been proposed. This approach comprises the use of optical nanoantennas for enhancing the absorption of pump laser radiation in the antenna gap, reducing the lifetime of photoexcited carriers, and improving the antenna thermal efficiency. This Review is intended to systematize the main results obtained by researchers in this promising field of hybrid optical-to-terahertz photoconductive antennas and photomixers. We summarize the main results on hybrid THz antennas, compare the approaches to their implementation, and offer further perspectives of their development including an application of all-dielectric nanoantennas instead of plasmonic ones.
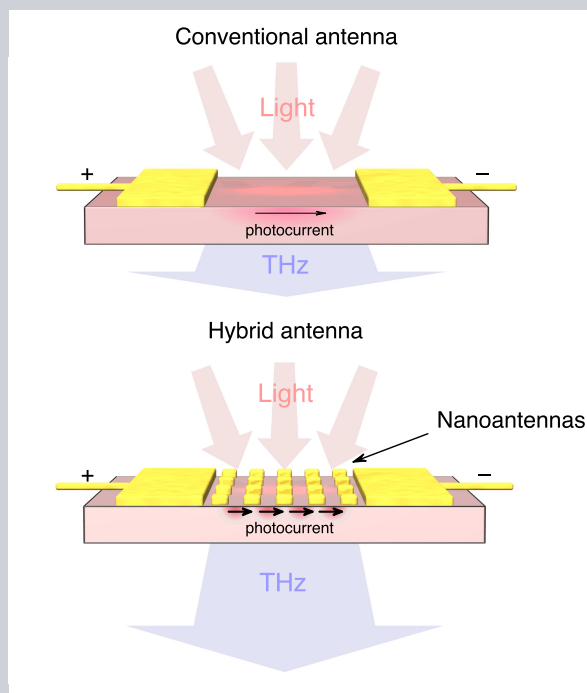
Enhancement of Terahertz Photoconductive Antenna Operation by Optical Nanoantennas

Sergey Lepeshov[1], **Andrei Gorodetsky**[1,2,*], **Alexander Krasnok**[1,3], **Edik Rafailov**[2], **and Pavel Belov**[1]

1. Introduction

The terahertz (THz) spectral range of electromagnetic waves (0.1–10 THz), lying between the microwave and optical regions, is of great interest, primarily due to the fact that in this band of the electromagnetic spectrum reside the frequencies of some elementary excitations in semiconductors and dielectrics [1–12], as well as rotational and vibrational resonances of complex, including biological, molecules [13–21]. As a result, THz waves have a tremendous number of applications in areas ranging from the detection of dangerous or illicit substances [6, 13, 22–27] and biological sensing [28–33] to diagnosis and treatment of diseases in medicine [20, 21, 34–41]. Moreover, this frequency band is of special importance for spectroscopy in astrophysics [42–47] because many astrophysical objects emit in the THz range of the spectrum. In addition, the THz technology is promising for wireless communication systems [48, 49] as a complementary technology to transmitters and receivers operating in high-frequency and microwave ranges, because it can potentially increase the speed of data transfer by hundreds of times [50–55]. Although, there are some reasonable hurdles, like strong absorption of THz waves by metals and water, on the way to the real life application of THz wireless technology to add bandwidth to mega- and gigahertz frequency devices [56–58], a significant progress has already been made [5, 59–61].

Until relatively recently, the generation of coherent THz waves was an extremely difficult task. However, research in semiconductors [7, 8, 62–66], and in the interaction of short (compared with all relaxation times) optical pulses with semiconductor and nonlinear materials (*photoconductivity effect* [67, 68]) stimulated the development of compact low-power ($\sim 10^{-14}$ J/pulse) THz radiation transmitters.

[1] ITMO University, St. Petersburg, 197101, Russia
[2] Aston Institute of Photonic Technologies, Aston University, B4 7ET, Birmingham, UK
[3] Department of Electrical and Computer Engineering, The University of Texas at Austin, Austin, Texas 78712, USA

[*] Corresponding author: e-mail: andrei@corp.ifmo.ru

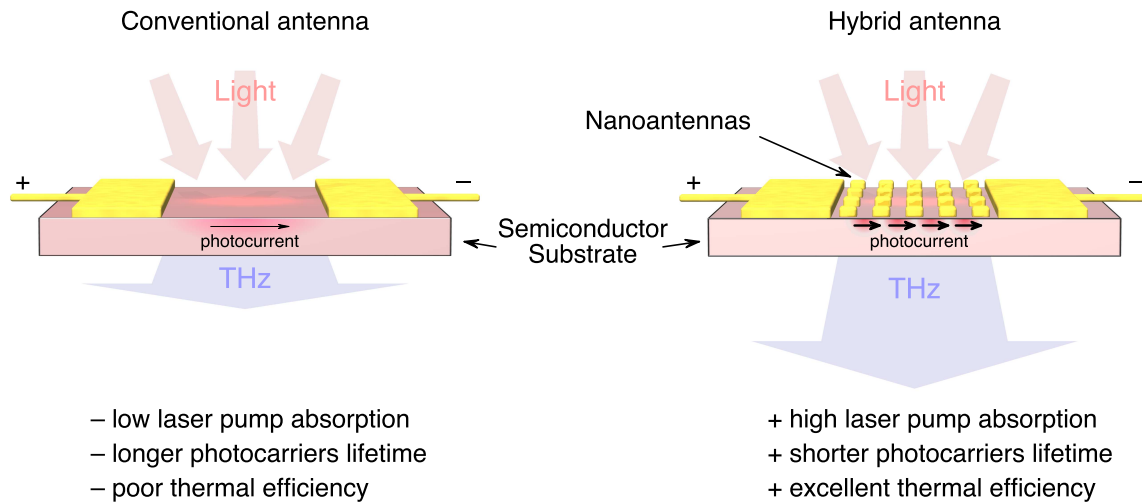Conventional antenna

Hybrid antenna

Figure 1 Illustration of the hybrid antenna advantages over conventional one.

Nowadays, the most common method for a low power THz generation by conversion of an optical pump involves the use of semiconductor structures with a surface conductivity [69, 70]. Two or more conductive electrodes spaced by a certain gap are deposited onto a semiconductor surface (Figure 1, left side). The electrodes are biased by the external voltage of several V. Such structure is referred to as *THz photoconductive antenna* if pumped by femtosecond (fs) optical pulses, or *THz photomixer* in the case of continuous (CW) pump by two lasers operating at close wavelengths with a difference being in the THz spectral range. Upon excitation the gap between the electrodes with a fs-laser, the concentration of charge carriers increases sharply for a short period of time, and the THz pulse generation occurs. The duration of this pulse and its spectrum are determined mainly by the carriers lifetime in the semiconductor. In the case of CW pumping, the carriers concentration changes with the difference frequency of pump wavelengths, and CW THz signal is emitted. The efficiency of such THz sources is strongly limited by the amount of the optical energy of laser radiation absorbed in the gap of the photoconductive antenna. Usually, this amount is rather small, taking into account the high values of the semiconductor refractive index at optical frequencies, leading to a high reflection coefficient. Moreover, the effectiveness of conventional photoconductive antennas is limited by low drift velocities of the photoinduced charge carriers in semiconductor substrates [71–73] and material breakdown threshold [74].

It has been shown recently, that the efficiency of the THz pulse generation can be significantly increased by placing so-called *optical nanoantennas* (NAs) [75–84] into the photoconductive gap (Figure 1, right side) [69, 70, 74, 85–90]. As a result, one gets an antenna comprising a comprehensive photoconductive THz antenna and an array of optical NAs. Such system can be called a *hybrid THz-optical photoconductive antenna*. These antennas are the result of the application of latest advances in nanophotonics area to THz sources technology for the purpose of their efficiency enhancement. The efficiency of the entire hybrid antenna is determined by the efficiencies of THz photoconductive antenna and an optical NA array and is usually higher by at least one order of magnitude than the efficiency of conventional THz antenna. Besides the pump field enhancement in the semiconductor substrate, the plasmonic NAs improve the thermal stability of the THz photoconductive antenna due to the large thermal conductivity of metals. As for detectors, the use of hybrid photoconductive THz detectors with optically resonant nanoparticles in the photoconductive gap allows for the enhancement of the near-field THz imaging resolution up to $\lambda/150$ [91]. This unprecedented resolution has become available due to the extremely high scattering provided by NAs into the semiconductor [i.e., low (< 200 C) temperature grown gallium arsenide (LT-GaAs)] detector surface layer and hence high enough concentration of carriers in the ultrathin semiconductor layer next to subwavelength detector aperture for evanescent THz field registration.

Another type of perspective THz detectors involves the use of plasmonic structures with resonances in THz frequencies [92–98], this technique can also be used for gaining THz spectrometers sensitivity through local field enhancement, however such devices wont fall within the scope of this Review.

This Review is intended to systematize all main results obtained by researchers in the field of hybrid optical-to-terahertz photoconductive antennas and photomixers. First, we just briefly describe the main operating principles of THz generation in photoconductive antennas and photomixers pumped with fs-optical pulses and double-wavelength CW laser radiation, since there is a great number of excellent reviews on this subject (among them, we recommend the following Refs. [6, 50, 62, 99–101]). Second, we discuss the general principles of operation of optical NAs and the prospects they offer for THz emission. We describe the plas-

mon monopole and dipole optical nanoantennas, two- and three-dimensional plasmonic gratings and features of their operation in hybrid THz antennas. Finally, we summarize and compare the main approaches to the implementation of the hybrid antennas, and give an outlook of further perspectives of their development including an application of all-dielectric NAs instead of plasmonic ones and the search for new materials.

2. Principles of THz photoconductive antennas and photomixers

2.1. Methods of coherent THz generation

One of the simplest, but perhaps not the most efficient, way to obtain the THz waves is by accelerated movement of the separated charge carriers in the surface field of a semiconductor under ultrashort light pulses [7, 67]. One of the physical mechanisms that drive the carriers inside a semiconductor is the *photo-Dember effect*. This effect consists in the formation of the electric field (and consequently a charge dipole) in the illuminated semiconductor due to the difference of electrons and holes diffusion velocities [102] under the strong absorption of optical excitation, which leads to an effective charge separation in the direction perpendicular to the semiconductor surface [103].

Another possible way to generate THz waves – *optical rectification* – works when a second order nonlinear media obtains a non-linear polarization under an intense optical radiation. It results in a polarization repeating the shape of the optical pulse envelope [104–106] or in the case of four-wave mixing in third-order nonlinearity, such as in THz generation via two-color laser-plasmas [107, 108], though the latter requires higher pulse energies produced by chirped pulse amplification [109].

Apart from these well-established methods, novel approaches of nanophotonics to THz generation that employ an artificial electromagnetic medium (*metamaterials and metasurfaces*) [110–118], and new types of materials (graphene [119,120], carbon nanotubes [121,122], and three-dimensional topological insulators such as Bi_2Se_3 [123]) have been recently proposed.

We should note here that the main competitors of photonic techniques for coherent THz radiation generation are all-electronic direct THz Quantum Cascade Lasers (QCLs) [124–126] and on-chip nonlinear semiconductor mixers of mid-IR QCL radiation [127, 128]. Monolithic design offers reasonable advantages over now table-top photonic setups, however, QCLs are extremely expensive in design and production, and direct THz QCLs operate only at cryogenic temperatures. In the scope of applications, QCLs will barely offer fine and continuous tunability, or generation of ultrabroadband THz signal, needed for spectroscopy. As a result, QCLs are geared mostly towards imaging, whereas photonic sources are especially demanded for spectroscopic applications. Development of antenna-based monolithic THz sources in conjunction with compact semiconductor lasers is also highly feasible [129].
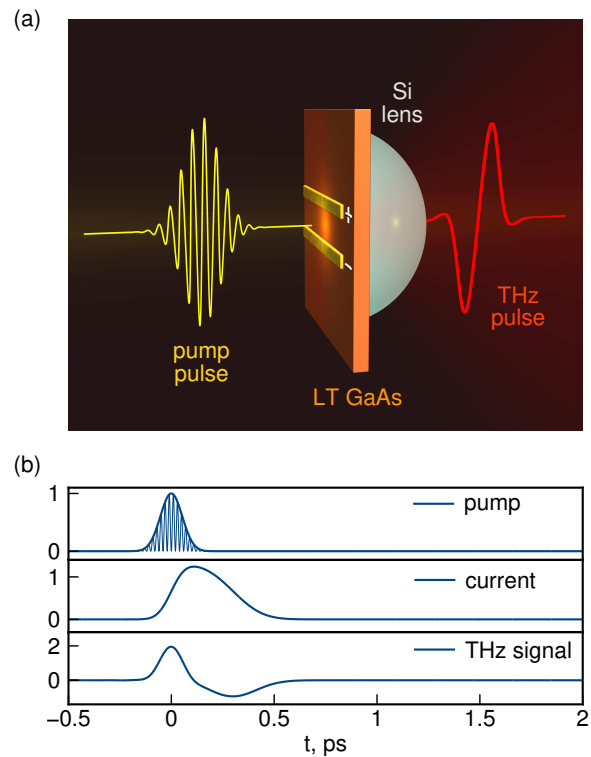

Figure 2 (a) Schematic view of a setup used to generate pulsed THz radiation by photoconductive LT-GaAs based antenna and (b) time evolution of pump radiation envelope, antenna photocurrent and generated THz signal.

2.2. Carrier dynamics in semiconductors under pulsed optical excitation

Currently, there are many different approaches to THz generation, in a vast variety of layouts and involving various materials. However, for practical applications, the method involving the excitation of non-equilibrium charge carriers in the surface layer of semiconductor structures by ultrashort optical pulses is the most widely used. Figure 2(a) shows the simplest layout for submillimetre waves generation in semiconductor (LT-GaAs) based photoconductive antennas. Fs-laser (usually Ti:Sapphire [6] or much cheaper fiber-based laser systems such as second [6] or fundamental [86, 89] harmonic of Er-doped fiber lasers) serves as a source of ultrashort light pulses with a duration of several tens or hundreds of femtoseconds. The shape of the optical pulse envelope is very important as it induces the nonlinear polarization of the same form (optical rectification), which is capable of increasing the output power of THz radiation [104, 105]. Silicon lens, shown in Figure 2(a), serves to collect and collimate the generated THz radiation [130,131] and at the same time as a heatsink to transfer heat excess away from the substrate. Moreover, it works as an anti-reflective element, since the refractive index of Si in THz range is equal to $n_{Si} = 3.4$ [132], which is about the same as one of high-resistive GaAs ($n_{GaAs} \approx 3.6$) [132].

The dependence of the output power of THz generation in a semiconductor P_{THz} on the frequency ω_{THz} is given by [133]:

$$P_{THz}(\omega_{THz}) \backsim \frac{1}{1 + (\omega_{THz}\tau_{eff})^2}, \qquad (1)$$

where τ_{eff} is the effective lifetime of photocarriers, equal to the lifetime of nonequilibrium charge carriers in the semiconductor. From the Eq.(1), it is clearly seen that the shorter the lifetime τ_{eff} is, the greater power P_{THz} can be obtained. Gallium arsenide grown by molecular beam epitaxy on a low-temperature substrate (LT-GaAs) is usually chosen as a photoconductive material, as this growth method allows obtaining a material with a larger number of defects and hence with shorter lifetimes of nonequilibrium charge carriers (≤ 200 fs [133]). When irradiated by fs-laser pulses with photon energies greater than the bandgap, the concentration of nonequilibrium charge carriers in LT-GaAs rapidly increases, and the electron-hole pairs are formed at the surface layer. In the semiconductor model, all electrons are set to have the same effective mass as they have a low energy because of the wide band of gallium arsenide. This model is not applicable to narrow-gap semiconductors such as indium arsenide (InAs). In the case of InAs, it is necessary to consider ensembles of equilibrium and photoexcited electrons interacting through self-consistent field [134], which greatly complicates the mathematical description of processes.

The localization of charges at surface states in the surface layer, gives rise to the so-called *built-in* field. The light-induced electrons and holes are accelerated and separated by this field, and the resulting uneven distribution of charge can be considered as a dipole with the dipole moment equal to the sum of momenta of all induced charges in the volume. The dipole oscillations occur until the equilibrium is established again. During the relaxation, electrons emit energy in the form of electromagnetic waves in the THz range and the relaxation time determines both spectrum and power of the generated radiation. Built-in surface field plays a very important role in this process. The stronger this field is, the more intense is the emitted THz signal. For this reason, biased metal electrodes are often applied to the semiconductor surface to create a stronger electric field. The mechanism of THz generation enhancement by such structures will be described in detail in the next section of this Review. Since the generation takes place near the air-semiconductor interface, a larger portion of the THz radiation is emitted into the GaAs substrate, owing to the the greater optical density. The reason for this is the greater optical density of the GaAs in comparison with air. Therefore, highly doped semiconductor materials are not suitable for efficient photoconductive antennas due to their increased absorption in the THz region of the spectrum [132]. On the other hand, the doping of the sample increases the concentration of photoinduced electron-hole pairs, which, ultimately, increases the current and hence the THz radiation power. A reasonable compromise between these competing factors (i.e. higher absorption vs. higher current) will substantially improve the efficiency of generation.

Another effective method of increasing the optical-to-THz conversion efficiency is the application of an external magnetic field. It has been shown, that a semiconductor placed in a constant magnetic field of 1 T generates THz radiation with efficiency up to 20 times larger than without magnetic field [135]. The optimal direction of magnetic field is the one perpendicular to the semiconductor surface, and THz pulse amplitude is proportional to the squared amplitude of the magnetic field. This effect is explained by the appearance of the *Hall component of the current*, excited carriers being driven by external or surface field [134–137]. However, such approach requires the use of expensive magnets that are not suitable for implementation in compact setups.

The analysis of temperature dependence of THz radiation power shows that with decreasing temperature the power goes up. With the GaAs temperature decreasing from 280 K down to 80 K, the radiation energy is increased by 3.4 times [138].

2.3. *Pulsed THz generation in photoconductive antennas*

An approach to THz generation in a semiconductor surface due to the accelerated motion of nonequilibrium charge carriers induced by fs-laser pulses and driven by semiconductor surface field, unfortunately, has low optical-to-terahertz conversion efficiency. To overcome these limits, metal electrodes (usually a nickel-gold-platinum alloy) are deposited onto the substrate surface and are biased with an external voltage to create a high electric field in the gap between them, where the photocarriers are generated, and thus enhancing the generation of the THz waves [139]. Such structures together with a photoconductive semiconductor substrate are referred to as *THz photoconductive antennas*. An example and principle of operation of such antenna are shown in Figure 2(a).

The mechanism of THz generation, in this case, is similar to that discussed in the preceding section. Under an ultrashort laser pulse, electron-hole pairs are formed in the surface layer. The conductivity of the semiconductor as a consequence increases proportionally to the electrons and holes concentration: $\sigma = qn_e\mu_e + qn_p\mu_p$, where q is the elementary charge, n_e (n_p) is the concentration of electrons (holes), and μ_e (μ_p) is their mobility. The increase of conductivity results in a giant current pulse of photoinduced charges, electrons and holes, being accelerated in opposite directions by the external electric field in the gap. The acceleration of charge carriers by the external field E_{bias}, in this case, can be described by the differential equation:

$$\frac{dv_{e,p}}{dt} = -\frac{v_{e,p}}{\tau_{eff}} + \frac{qE}{m_{e,p}}, \qquad (2)$$

where $v_{e,p}$ is the drift velocity of electrons and holes, $m_{e,p}$ are their masses, τ_{eff} is approximately 30 fs in low-temperature GaAs, E is the local field. The latter is related to
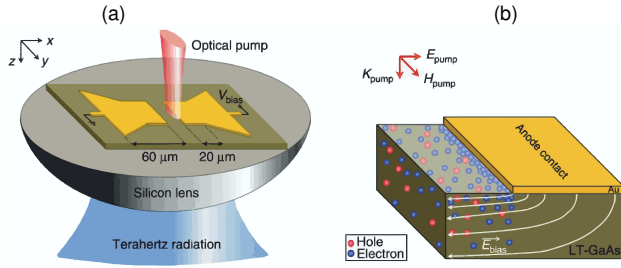
Figure 3 (a) A photoconductive antenna consisting of a GaAs substrate and electrodes arranged in the bow-tie geometry. (b) The distribution of photoinduced electrons near the anode when the bias voltage is applied to the electrodes. [70]

E_{bias} by $E = E_{bias} - \frac{P}{\alpha\varepsilon_0}$, where α is the static dielectric susceptibility of semiconductor (equal to 3 for the LT-GaAs), ε_0 is the vacuum permittivity, and P is the polarization caused by the separation of electrons and holes, which gives the bias threshold of the LT-GaAs of 300 kV/cm. The time evolution of the polarization can be described by the following inhomogeneous differential equation:

$$\frac{dP}{dt} + \frac{P}{\tau_{rec}} = J(t), \qquad (3)$$

where τ_{rec} is the recombination time of holes and electrons, and J is the density of currents on the surface of the semiconductor defined by: $J(t) = qn_e v_e + qn_p v_p$. From Eqs. (2-3), using Maxwell's equations, one can derive a formula for the intensity of the radiated THz field at a much larger than THz wavelength λ distance z from the source [140]:

$$E(z,t) = -\frac{A}{4\pi\varepsilon_0 c^2 z} \cdot \frac{dJ}{dt} = -\frac{A}{4\pi\varepsilon_0 c^2 z} \cdot (qv\frac{dn}{dt} + qn\frac{dv}{dt}), \qquad (4)$$

where n is the total concentration of carriers, v is their velocity, A is the area of the irradiated surface (equal to the area of the gap between the electrodes), and c is the speed of light in a vacuum. Thus, the external field increases the energy of charge carriers, and hence the output power of THz radiation, not influencing, however, the spectral characteristics, as they are determined by the lifetime of electrons and holes. Pump pulse envelope, photocurrent in the surface layer, and resulting THz field examples obtained with this model are shown in Figure 2(b).

Authors of Refs. [70, 141] have observed that various pump of the semiconductor in the THz photoconductive antenna gap can affect the output power. Moreover, there are two options for photoconductor pump: uniform illumination of the antenna gap, and partial asymmetric illumination close to the anode (Figure 3(a)). In the case of uniform illumination, the current of photoinduced charge carriers is proportional to the optical power of the pump. However, in the case of asymmetric illumination, the photocurrent and hence the THz signal are increasing nonlinearly with the optical pump power. This pumping regime is characterized by the increased electric field near the anode, and, conse-
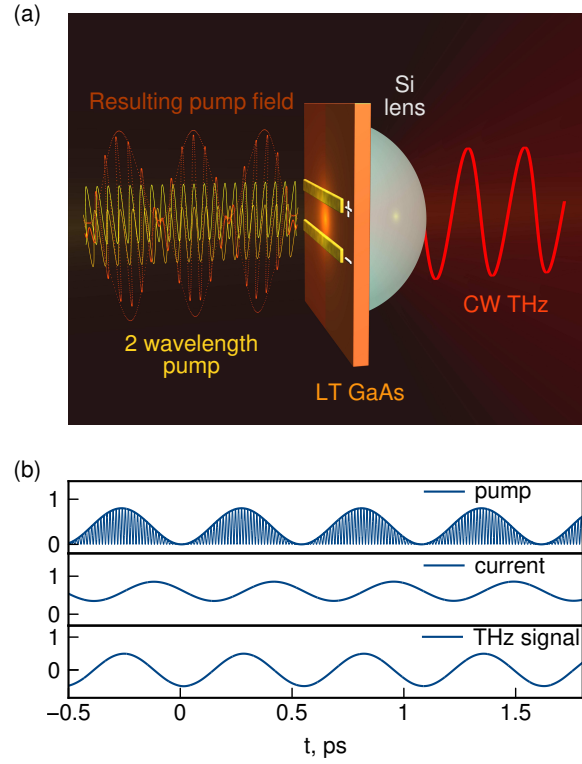

Figure 4 (a) Schematic illustration of CW THz generation by a LT-GaAs based photomixer and (b) time evolution of pump radiation envelope, antenna photocurrent and generated THz signal.

quently, increased electrons concentration in this region (Figure 3(b)). This leads to an increase of the photocurrent, resulting in an enhanced power of the THz signal. It has been reported that the asymmetric illumination of the photoconductive antenna gap gives more than 4-fold enhancement compared to the uniform illumination [141]. Moreover, it has been shown that the stronger optical field is concentrated in the area of the anode, the more powerful THz radiation is [142].

2.4. Continuous THz generation in photomixers

The process of THz heterodyne generation in semiconductors is similar to that discussed in the preceding sections, the only difference being the pump laser regime. Under continuous double-wavelength pump with a frequency difference lying in the THz region, electron-hole pairs are formed in the surface layer and the conductivity of the semiconductor is modulated proportionally to the electrons and holes concentration. Such devices for photoconductive CW THz generation are usually called *photomixers* [143, 144]. The schematic layout of CW THz generation in a photomixer and its principle of operation are shown in Figure 4(a).

The surface conductivity and charge carriers acceleration in a photomixer are similar to those in a photoconductive antenna, and the number of carrier pairs similarly
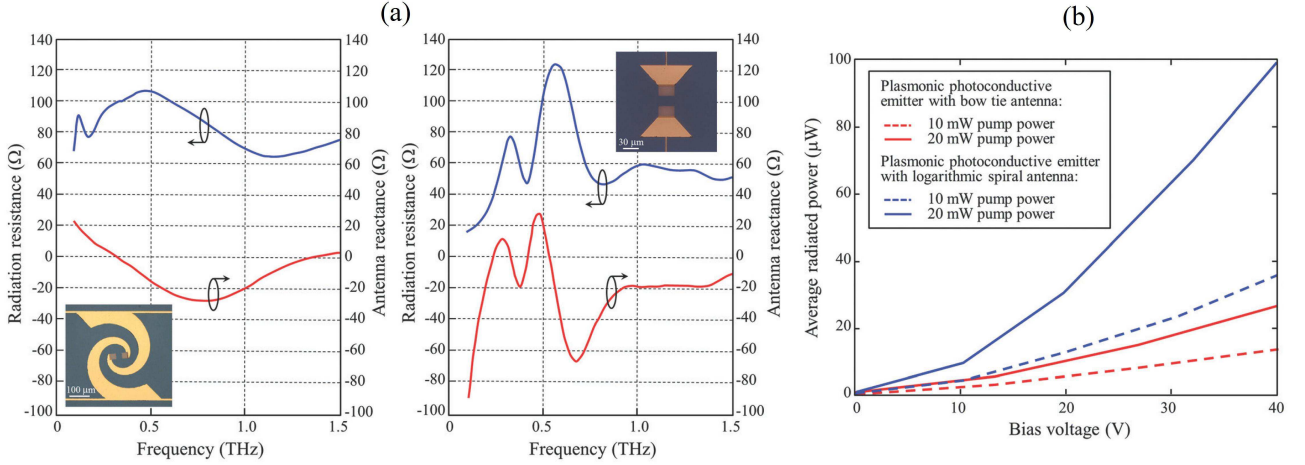
Figure 5 (a) The frequency dependence of impedance (blue) and reactance (red) of two different THz antennas, spiral and bow-tie, respectively. (b) Dependencies of the radiated power of the spiral (blue) and bow-tie (red) antennas on the bias voltage between electrodes for different powers of fs- pump. [88]

follows the pump evolution:

$$\frac{dn(t)}{dt} = \frac{\eta I_{\text{pump}}(t)}{h\nu} - \frac{n}{\tau_{\text{rec}}}, \qquad (5)$$

where η is the external quantum efficiency, $I_{\text{pump}}(t)$ is the pump intensity, τ_{rec} is the carrier recombination time, and $h\nu$ is the energy of the pump photon.

The pump radiation in the case of photomixing comprises two laser beams bringing to the surface average intensities I_1 and I_2 at the frequencies ω_1 and ω_2, respectively. Thus, the intensity at the surface can be described as:

$$I_{\text{pump}}(t) = I_1 + I_2 + 2\sqrt{I_1 I_2}\left(\cos\left(\omega_1 - \omega_2\right)t + \right.$$
$$\left. + \cos\left(\omega_1 + \omega_2\right)t\right). \qquad (6)$$

The second oscillating term in the sum changes within a timescale that is significantly shorter than the carrier effective recombination time τ_c, hence not affecting the photocurrent. Neglecting this term, after substitution of Eq. (6) into Eq. (5), one obtains the evolution of carrier density [143]:

$$n(t) = \frac{\eta \tau_{\text{rec}}}{h\nu}\left(I_1 + I_2 + \frac{\sqrt{I_1 I_2}\sin\left(\omega t + \phi\right)}{\sqrt{1 + \omega^2 \tau_{\text{rec}}^2}}\right), \qquad (7)$$

where $\omega = (\omega_1 - \omega_2)$ is the THz frequency, and $\phi = \tan^{-1}\left(\frac{1}{\omega \tau_{\text{rec}}}\right)$ is the phase delay due to the carriers lifetime.

Since the applied field is constant, for the photocurrent we obtain [145]

$$J(t) = I_D + \frac{I_A}{\sqrt{1 + \omega^2 \tau_{\text{rec}}^2}}\sin\left(\omega t + \phi\right), \qquad (8)$$

where $I_D = E_{\text{bias}}\mu_e \tau_{\text{rec}}(I_1 + I_2)$ is the DC photocurrent and $I_A = 2E_{\text{bias}}\mu_e \tau_{\text{rec}}\sqrt{I_1 I_2}$ is the AC component of the current,

which is responsible for the generation of the CW THz signal:

$$E_{\text{THz}}(t) \propto \frac{dJ(t)}{dt} = \frac{\omega I_A}{\sqrt{1 + \omega^2 \tau_{\text{rec}}^2}}\cos\left(\omega t + \phi\right). \qquad (9)$$

It can be seen, that for the maximum conversion efficiency, the powers of both wavelength modes should be as close to each other as possible. The pump intensity profile, the corresponding photocurrent, and far field THz signal of the photomixer calculated with the described model are shown in Figure 4(b).

2.5. *Effect of the contact electrodes shape on the radiative characteristics of THz photoconductive antennas and photomixers*

One of the most important characteristics of all antennas, including radio, microwave, and THz photoconductive ones, is the amount of emitted power. However, between the radio or microwave antenna and THz photoconductive one, there is a significant difference – the nature of the input signal. In the case of a THz antenna, it is the laser radiation that generates the nonequilibrium electrons and holes in the surface layer of the photoconductor. Therefore, the THz photoconductive antenna is usually considered as a system consisting of two elements: the photoconductor and the antenna. These elements, in turn, are described by the traditional physical quantities, such as active and reactive conductivity, capacitance, and input impedance [133, 141].

The output power P_{rad} of THz photoconductive antenna can be expressed in terms of antenna resistance and reactance [141]:

$$P_{\text{rad}}(\omega) = \frac{1}{2}|S_{\text{p}}(\omega)P_{\text{opt}}(\omega)|^2 \xi \frac{G_A}{(G_A + G_{\text{p}})^2 + (\omega C + B_A)^2}, \qquad (10)$$

where S_p is the current susceptibility of the photoconductor, $P_{opt}(\omega)$ is the optical pump power at frequency ω, ξ is the antenna efficiency (which describes the dissipative losses in the antenna material [146]), G_A and B_A are respectively the active and reactive conductances of the antenna, G_p is the conductivity of the photoconductor, and C is its capacitance. Regardless of the THz photoconductive antenna geometry, in order to maximise its radiated power, its stray conductance must be much less than its active conductance $(\omega C + B_A) \ll (G_A + G_p)$. Full or partial compensation of reactive conductance can be achieved by maintaining the inductive load of the antenna at the same level as the capacitive load of the photoconductor, or by adding a negative reactive conductance shunt into the antenna [147, 148].

In a number of works [86, 87, 149–151] it was observed that the geometry of electrodes affects both the spectrum width and the frequency of the maximum THz radiation intensity. Usually, the electrodes of THz antennas have the geometry of dipole, logarithmic, spiral, and bow-tie antennas [152–155]. The consideration of the real antenna geometry can be done numerically or experimentally. In Ref. [88] a comparative analysis of two common THz antenna geometries, spiral and bow-tie, is performed. Figure 5 shows the dependence of radiation resistance and reactance of these antennas on the frequency (a) and the dependence of the radiated power on the bias applied to electrodes for THz frequency corresponding to the maximum output power (b). It can be seen that the spiral antenna, having a larger radiation resistance and a smaller reactance, emits more effectively than the bow-tie antenna within a wider frequency range. Thus, the maximum active resistance and the minimum absolute value of the reactive resistance are prerequisite for efficient THz radiation generation and can be adjusted by choosing of the antenna geometry [153, 156].

Since active and reactive resistances affect the power emitted by a THz antenna, the spectral characteristics of the antenna impedance and reactance determine the spectral characteristics of the THz signal. It has been observed that the antenna with radiation resistance slightly depending on frequency in the THz range has a wider frequency range of an effective operation [88, 157]. The spiral and bow-tie geometries discussed above are examples of such antennas. Figure 6 shows the spectrum of THz signal from the spiral photomixer antenna (white squares) measured by a bolometer. At frequencies between 0.1 and 0.6 THz the signal power is almost constant [133]. On the other hand, antennas with a pronounced resonant impedance, such as full-wavelength dipole antennas (black squares), have narrow-band emission spectrum [147, 158, 159].

In Ref. [151] the bow-tie THz antennas made in the form of Sierpinski triangles are studied. The results are shown in Figure 7. Due to the presence of subwavelength triangle holes on the antenna surface, the strong plasmon resonances at the frequencies of the antenna radiation are excited. Owing to the special distribution of surface plasmon currents, these THz fractal antennas have a higher performance than the standard bow-tie antenna. The increasing of fractal degree leads to the enhancement of the number of
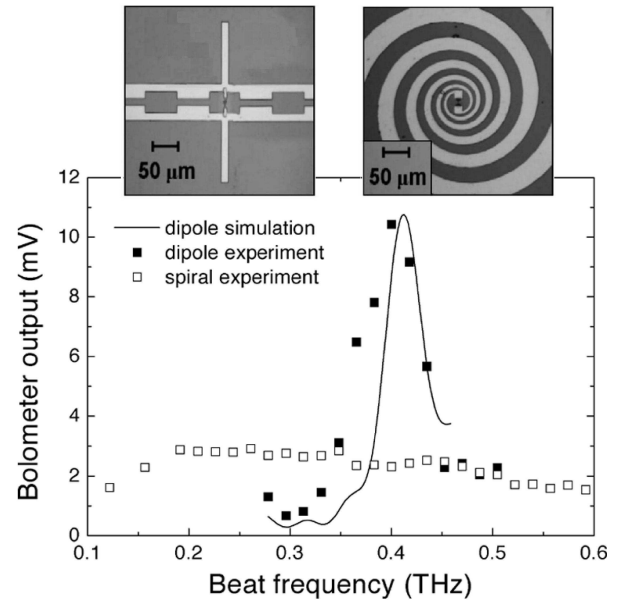

Figure 6 The frequency dependence of the output bolometer signal for the spiral and full-wavelength dipole THz photomixers. Dots represent experimental data, solid lines - numerical calculations. [133]

plasmon resonances and ultimately to the enhancement of the radiated power.

3. Hybrid photoconductive THz antennas

3.1. Advantages of optical nanoantennas for THz antennas

Optical NAs possess all the inherent characteristics of their radio and THz counterparts, except of course that they operate with fields in the optical spectral range. The dimensions of NAs are typically of the order of several hundreds of nanometers. Today, the most widely used and well-studied NAs are the plasmonic ones. They are applied extensively in devices that use photon-electron conversion, such as photodiodes, LEDs, and photovoltaic converters [77, 78, 160, 161]. Recently, a number of papers has demonstrated the enhancement of the optical-to-terahertz conversion efficiency in THz photoconductive antennas with plasmonic NAs. Here we consider the benefits of the optical NAs from the perspective of application for hybrid THz antennas.

To understand the advantage of optical NAs for THz photoconductive antennas, let us recall that the radiated THz field amplitude is proportional to photocurrent density [see Eqs.(4) and (9)]. The photocurrent depends on the density of carriers that is a function of time, carriers mobility, and the bias field. It is needed to maximize the photocurrent density to enhance the THz field generated by the photoconductive antenna. However, the bias field and charge density are
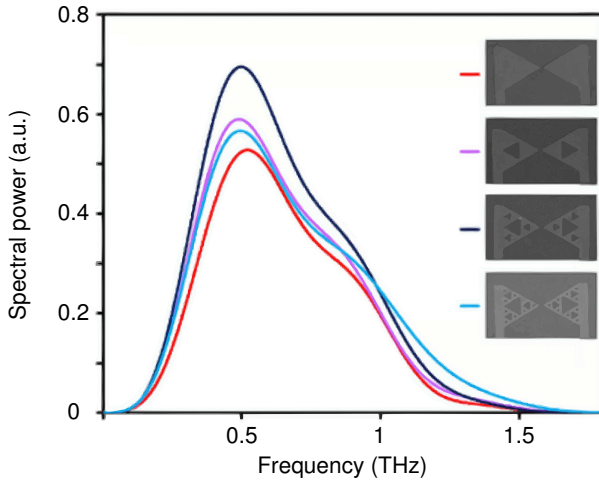
Figure 7 The THz power spectra for the bow-tie antennas of different fractal degree. [151]

Figure 8 Numerically calculated electric field distribution profiles at the interface between air and the GaAs substrate (a) without and (b) with a silver nanoparticle. Densities of the power absorbed in the GaAs substrate (c) without and (d) with a silver nanoparticle.

limited by the material breakdown, charge screening, and thermal damage factors. Recently it has been demonstrated that these factors can be considerably improved with the application of optical NAs. The benefits of the optical NAs application including a strong electric field enhancement within semiconductor substrate, reducing the carrier screening effect, and thermal stability enhancement we discuss below.

Strong electric field enhancement. An optical NA, as a part of a hybrid THz-optical photoconductive antenna or photomixer, converts the pump optical radiation into a strong near-field distribution and redistributes the energy within the semiconductor layer. The enhancement of an electric field is described by the local field enhancement factor:

$$\delta = \frac{|E|}{|E_0|}, \qquad (11)$$

which describes by which factor the modulus of the electric field $|E|$ is increased locally (i.e. at a certain point) in the presence of a NA compared to its value $|E_0|$ in the absence of the NA.

The local electric field enhancement occurs due to the plasmon resonance of the NA [69, 87, 160–162]. At the same time, the plasmon resonance excited in the metal NA asymmetrically scatters the incident wave, and the field is redistributed in the semiconductor substrate so that the local electric field enhancement factor near the electrodes becomes much greater than the electric field of the incident wave. Therefore, the optical power absorbed by the semiconductor P_{opt} in the volume V:

$$P_{opt} = \frac{1}{2} \int \sigma \delta^2 |E_0|^2 dV \qquad (12)$$

increases proportionally to δ^2. Here, the value σ is a medium conductivity. As a result, the concentration of nonequilibrium charge carriers near the electrodes $n_{e,p}$ increases, and hence the efficiency of optical- to-terahertz
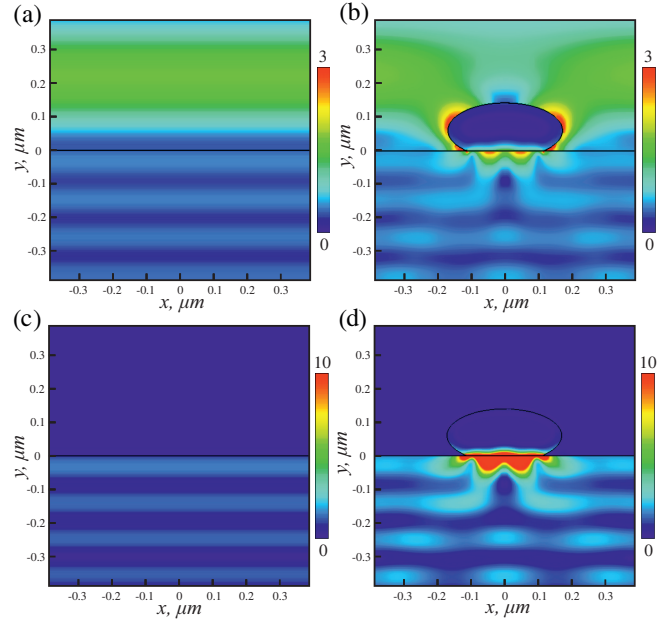
conversion increases too, according to Eqs.(4) and (9). The physical dimensions and material of the NAs play an important role in the excitation of the plasmon resonance and the electric field enhancement in the substrate.

As an example, we bring the results of numerical calculations of the electric field distribution at the air-GaAs interface with a Ag spheroid NA and without the NA, which are presented in Figures 8(a,b). The results are obtained by means of the software package CST Microwave Studio. The structure is excited by normally propagated plane electromagnetic wave with the wavelength of 800 nm. The geometrical parameters of the NA correspond to the optimal ones for the excitation of plasmon resonance in such structure at the wavelength of 800 nm. The large semi-axis of the spheroid is a=170 nm, minor semi-axis of the spheroid is b=100 nm. The magnitude of the electric field under the NA (Figure 8(b)) is in about 3 times larger versus the case of the NA absence (Figure 8(a)). Figures 8(c,d) show the distributions of absorbed power densities in the GaAs substrate with and without Ag nanoantenna. It is clearly seen that the power absorbed inside the GaAs in the presence of silver NA is significantly larger (in ten fold) than without the NA.

Reducing of the carrier screening effect. The effectiveness of conventional photoconductive THz antennas is strongly limited by low drift velocities of the photoinduced charge carriers in semiconductor substrates [71–73]. For an efficient optical-to-terahertz conversion in the frequency range above 0.5 THz, the carriers relaxation time τ_{rel}, as discussed earlier in Section 2 must be subpicosecond. Ac-

cording to the formula $l = v_{e,p} \tau_{rel}$, the mean free path l is about 100 nm. Therefore, only a small part (about 5% [70]) of nonequilibrium electrons and holes reaches the electrodes and participate in the efficient THz generation. The rest of the charge carriers recombines with charges of opposite sign on the way towards the electrodes. This effect is called *carrier screening effect* [71, 73]. The diffraction limit for electromagnetic waves does not allow focusing the laser pump into the spot of 100 nm. Therefore, in order to reduce the effect of screening and to improve the properties of photoconductive antennas, optical NAs are used [81].

Thermal stability enhancement. The excess of heat in conventional THz antennas leads to the thermal generation of carriers after optical pulse excitation [163]. Recombination of thermal and photoinduced carriers in subsequent cycles of charge carriers generation prevents the stable operation of the photoconductive antenna. Recently it has been shown that the optical NAs embedded in a THz photoconductive antenna can improve the thermal stability of the latter due to the large thermal conductivity of metals [74]. For example, gold has the thermal conductivity of 3.14 W/cm·K that is six times larger than the thermal conductivity of GaAs (0.55 W/cm·K). Such higher thermal efficiency also makes the optical NAs very attractive for use in THz sources.

Thus, the optical NAs being embedded in a THz photoconductive antenna can maximize the transfer of light energy into the absorptive semiconductor substrate and minimize the path length of charge carriers traveling between metallic electrodes. As a result, the optical NAs enhance the performance of the photoconductive THz antennas. Below, we review the most recent works and organise them according to the approach to optical NA realisation.

3.2. Plasmon monopole nanoantennas

The simplest type of NAs applied for hybrid THz antennas is monopole one. The monopole NAs are able to provide a strong electric field enhancement of laser radiation in their vicinity [77]. The optical properties of such NAs dependent on their size, shape and material. Thus, they can be easily tuned to any optical wavelength of operation. The arrays of the monopole NAs can be easily fabricated by means of chemical technics or thermal dewetting [164] even in the gap of THz photoconductive antennas.

The authors of [165] propose silver plasmonic monopole NAs in the form of so-called *nanoislands* (Figure 9(a)). The fabrication of such monopole NAs is done by thermal evaporation of silver (Ag), with subsequent deposition onto LT-GaAs antenna substrate surface. This method can be used to pattern nanostructures inside a large area, because of lower costs compared to, for example, electron beam lithography used for the precise fabrication of metal nanostructures [166]. Silver in the hybrid THz-optical antenna is used due to the high quality factor of the silver nanostructures in the visible range, which allows for achieving maximum localization of the field in the semiconductor surface layer with minimal dissipated losses of NAs. In addition, Ag has a relatively low melting temperature, and
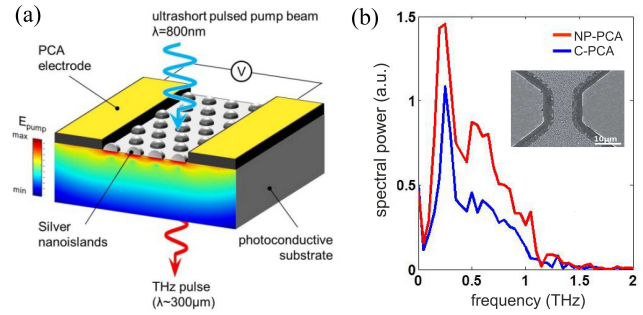

Figure 9 (a) Schematic representation of the photoconductive THz antenna with a large area of the silver nanoislands (monopole NAs). (b) The power spectra of the THz radiation for the conventional photoconductive antenna (C-PCA) and hybrid photoconductive antenna (NP-PCA) THz photoconductive antennas. Inset: the SEM image of the silver nanoislands. [165]

therefore its thermal evaporation is possible without thermal damage to the semiconductor GaAs substrate [167]. The geometrical parameters of the monopoles are specially derived so that the plasmon resonances are excited in the structure under an optical pump. For a pump radiation of 800 nm wavelength, which is typical for Ti:Sapphire fs-lasers, nanoislands should have a thickness of 20 nm and a diameter of 173 nm.

Figure 9(b) compares the emission characteristics of a conventional THz photoconductive antenna and of a hybrid optical-THz antenna containing nanoislands. It is clearly seen that the hybrid structure has a 1.5-2 times higher conversion efficiency, particularly enhancing the high-frequency part of the generated spectrum. This can be explained by Eq.(4): the monopole NAs concentrate the light within the gaps of adjacent nanoparticles, so that the absorption of optical radiation in these areas increases, growing the concentration of nonequilibrium carriers $n_{e,p}$, which increases the amplitude of the output THz signal E_{THz}. However, this field redistribution leads to a decrease in its value in the vicinity of nanoislands and significantly reduces the density of electrons and holes in these areas. Nevertheless, this does not affect the total current of photoinduced charges, as silver monopoles are almost perfect conductors for an external electric field. This process is described in detail in Refs. [81, 165].

Another possible realization of hybrid THz antennas is an array of rectangular monopole NAs arranged inside the photoconductive gap of photoconductive antennas and photomixers [168]. Figure 10(a) schematically shows a hybrid THz antenna with an array of rectangular nanostructures as well as a SEM image of these nanostructures. The nano-pattern consists of AuGe squares having a diagonal of 500 nm and a lattice period of 600 nm. This nano-pattern is incorporated in the THz antenna on the SI-GaAs region between the two electrodes. The mechanism of optical local field enhancement in the vicinity of these NAs is similar to the one in previously described, namely the plasmon resonance excitation. This structure has been realized utilizing
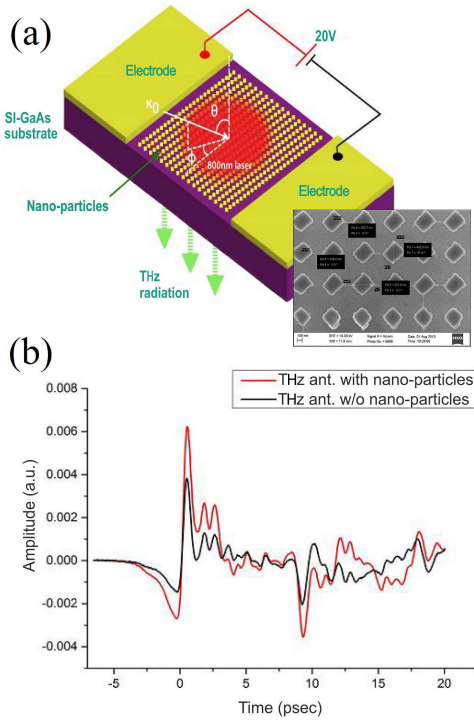
Figure 10 (a) Hybrid THz-optical photoconductive antenna with an array of monopole NAs. The array is fabricated on a substrate of semi-insulating GaAs (SI-GaAs). (b) Output signal of THz photoconductive antennas with (red curve) and without (black curve) monopole nanostructures. [168]

the electron beam lithography. This nanostructured hybrid THz-optical photoconductive antenna is able to double the emitted THz power in comparison with conventional photoconductive antennas (Figure 10(b)).

In Ref. [74], the hybrid THz antenna with hexagonal metal nanostructures has been proposed and realized. It has been shown that these antennas are superior to plasmonic nanorods-based ones (described below) in THz generation enhancement. Figure 11(a) shows an array of such monopole NAs fabricated inside the photoconductive gap of a dipole THz antenna using focused ion beam technology. It is known that the increase of pumping intensity increases the photoinduced current, which leads to heating of the semiconductor substrate and eventually to its thermal breakdown [169, 170]. It has been shown, that an important property of these THz photoconductive antennas with integrated hexagonal NAs is their high resistance to thermal breakdown [74]. Figure 11(c) demonstrates the advantage of the hexagonal NAs over grating NAs and conventional THz antennas. To achieve similar photoinduced currents, different antennas require the application of different biases between the electrodes. Moreover, maintaining a predetermined value of the current in the structure with hexagonal monopoles requires less external stress than in other antenna realizations. This suggests that conventional antennas and plasmonic gratings generate more heat than hexagonal NAs, and, accordingly, have a greater risk of experiencing thermal breakdown [74]. Figure 11(d) shows the dependence of radiated THz power on the average power of the fs-laser pump. When comparing the grating and hexagonal NAs, the superior performance of the latter is clearly seen. This is due to a combination of the external field generated by the electrodes, and localization of photoinduced charges in the vicinity to the hexagons tops (Figure 11(b)).

3.3. Plasmon dipole nanoantennas

The dipole NAs consist of two monopole ones arranged close to each other [175]. Such structures provide a stronger field localization in the gap between the nanoparticles and larger values of the absorbed power. The metal dipole NAs are used in THz photoconductive antennas and photomixers, enhancing an optical field of pump laser and redistributing it into the surface layer of the semiconductor substrate near the electrodes. The first implementation of dipole NAs embedded inside the gap of THz antenna are interdigitated nanostructured electrodes, or as they often called, "nano-fingers" [86, 144, 147, 176–178]. Figure 12(a) presents a interdigitated nanostructures embedded in the gap between the electrodes of the logarithmic photomixer. THz photomixers with such nanostructures feature lower parasitic capacitance and, consequently, lower reactance if compared with conventional THz photomixers, as well as higher optical field localization inside the working area of the antenna (see Figure 12(b)). Hence, photomixers with nanostructured dipole antennas in the photoconductive gap are more effective sources of CW THz radiation [133] if compared to microstructured ones. In some works [171, 172], it has been shown that with increasing the number of dipoles (fingers), the optical-to-THz conversion efficiency increases (Figure 12(c)). This dependence can be explained by the smaller distance between the dipoles in THz photomixer with a greater number of fingers, hence increased the degree of the optical field localization in the gap and decreased the effective lifetime of photoinduced charge carriers.

An updated approach to the design of the embedded dipole NAs is the so-called dipole tip-to-tip NAs [173, 174, 178]. Two most commonly used realizations of such nanostructures embedded in a THz photomixer are shown above. On one side conventional rectangular dipole nanoparticles are shown and trapezoidal bowtie NAs on the other (see Figure 13(a)). Being a continuation of the metal electrodes, these tip-to-tip NAs are designed to reduce the path length of photoinduced electrons and holes [175]. Moreover, due to the nanoscale gap between the dipoles, tip-to-tip NAs enhance the localization of the external optical field [173, 178, 179]. High localization of the field in the gap (see Figure 13(b), left picture) occurs because of the surface plasmon excitation due to plasmon resonance at the antenna excitation wavelength [175]. This increases a laser radiation absorption in the semiconductor substrate within the gap, and, consequently, the concentration of charge carriers in the gap. The rapid increase in the charge carriers concentration leads to a huge impulse of the photocurrent that is much greater than in conventional THz antennas.
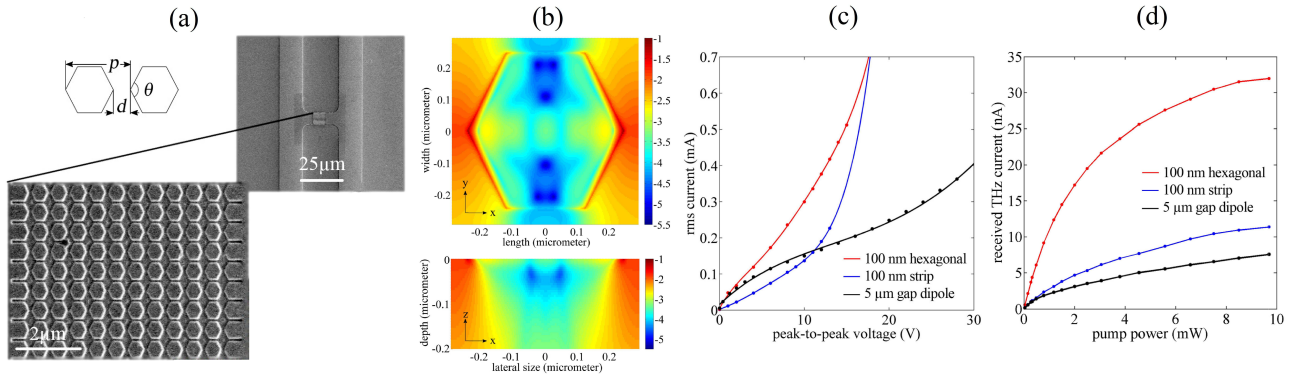
Figure 11 (a) SEM image of periodic array (with period p) of hexagonal NAs arranged on a SI-GaAs substrate. (b) Electric field distribution profile near the hexagonal NA. (c) Peak-to-peak voltage dependence of photo-excited current in the hybrid THz antenna with hexagonal NAs (red curve), strip plasmonic gratings (blue curve), and the conventional dipole antenna (black curve). (d) Comparison of received THz currents from the hybrid THz antennas with hexagonal monopoles, strip plasmonic gratings, and conventional dipole antenna in depends on the pump optical power. [74]

The amplitude of THz radiation is directly proportional to the rate of change of the photocurrent density, according to Eq.(4), so THz dipole antenna with integrated optical NAs demonstrate higher output power of THz signal than conventional one at the same pump rate, only because of such nanoscale extensions of the electrodes (Figure 13(c)).

In Ref. [174] it has been noticed, that due to lower capacitive reactive resistance, receiving ability of the bow-tie antenna is much better than one of the rectangular-shaped NAs, as a result, the degree of the optical field localization in the trapezoidal NA gap is significantly higher (Figure 13 (c), right picture) [174]. In addition, a smaller capacitance increases the efficiency of generation of THz radiation by such antenna [133].

3.4. Two-dimensional plasmonic gratings

Numerous researchers [70, 81, 85–89, 150, 180–182] have shown that on of the most effective implementation of dipole

Figure 12 (a) Spiral THz photomixer with built-in finger NA. (b) Electric field distribution in finger nanostructure of THz photomixer. (c) Comparison of the radiated power in nanostructured THz photomixers with a different number of fingers. [171–173]

NAs in the THz photoconductive antennas and photomixers are arrays of metal dipoles whose length is of the order of the gap size between the electrodes. Arrays of dipole plasmonic NAs have received the name of plasmonic gratings or plasmonic nanorod gratings [81].

Figure 14(a) shows the bow-tie THz photoconductive antenna with embedded plasmonic gratings. Usually, the penetration of light through the apertures is limited by the diffraction limit. However, the geometrical parameters of the gratings can be chosen so that the radiation of a fs-laser with a wavelength of 800 nm excites the surface plasmon wave in this periodic structure. The excitation of plasmon waves allows the transfer of the most part of the optical pump energy into a semiconductor substrate [183]. The surface plasmon greatly enhances the intensity of the optical field near the metallic electrodes (Figure 14(b)), as a result, the path length of photoinduced electrons and holes to the anode and cathode is reduced in comparison with conventional THz antennas (Figure 2).

The optical properties of this structure are very sensitive to the polarization of the incident light. When the electric field of the optical pulse is parallel to the plasmonic lattice nanorods, the reflection from the grating surface is sufficiently large. On the contrary, in the case of perpendicular orientation of the electric field vector and nanorods, maximum conversion of incident light into plasmon waves is achieved [81].

The authors of [180] suggest to use unincorporated plasmonic grating in the gap of THz photoconductive switch for enhanced THz pulse generation (Figure 15(a)). Such metal strips of the grating can reduce electrons lifetime in a semiconductor. Antenna and NA were fabricated on a GaAsBi semiconductor substrate characterized with a shorter carrier lifetime than the LT-GaAs substrate [184]. It is shown that when using this structure, more than 2-fold increase of the amplitude of THz signal can be achieved (see Figure 15(b)). However, conversion enhancement in this type of plasmonic
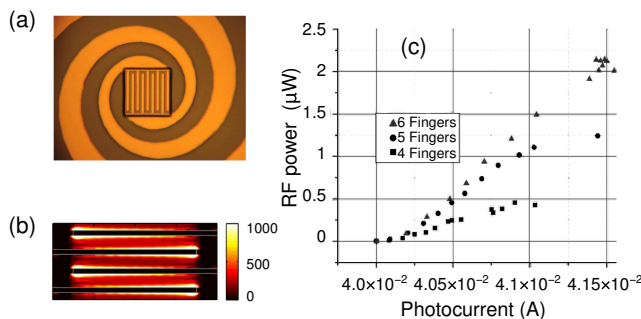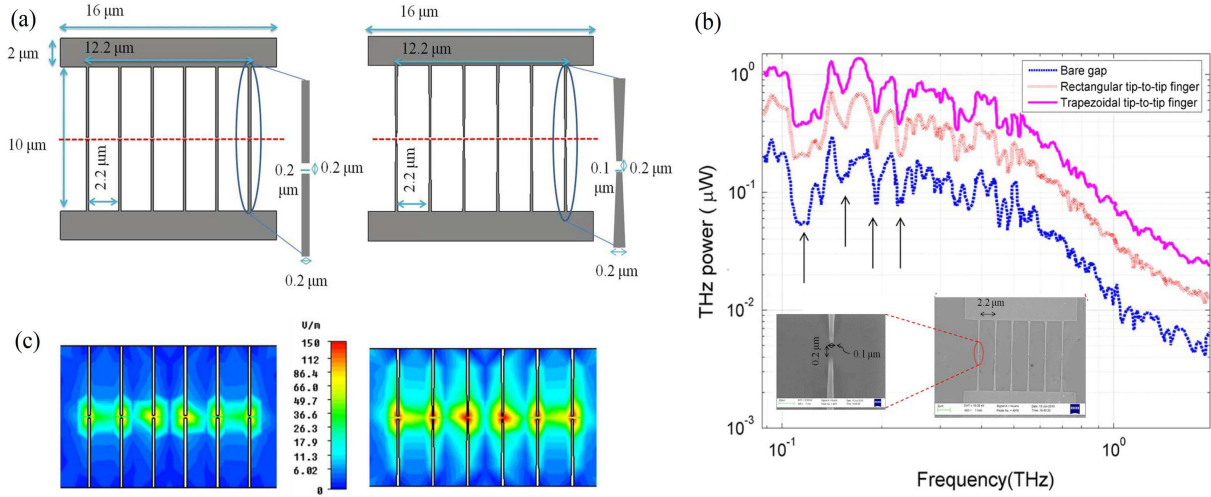
Figure 13 (a) The geometry and (c) electric field distribution profiles of rectangular (left) and trapezoidal (right) dipole NAs embedded in a THz photoconductive antenna. (b) The spectra of the THz radiation power for hybrid-optical photoconductive dipole antennas with built-in trapezoidal and rectangular NAs and conventional THz photoconductive antenna. [174]
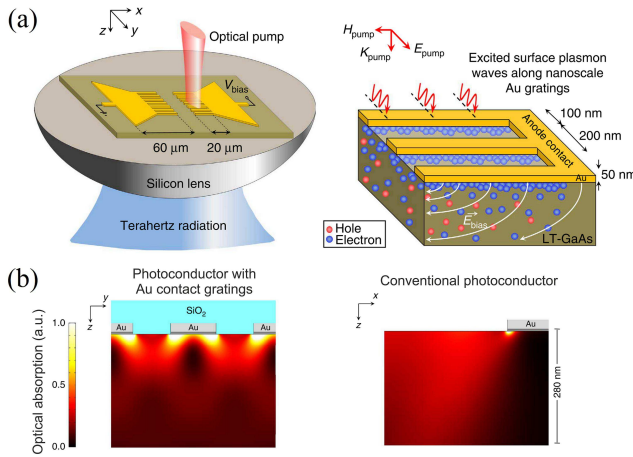

Figure 14 (a) The geometry of the hybrid THz-optical photoconductive antenna and the distribution of electrons and holes near plasmonic nanorods. (b) The image of the distribution of absorbed optical energy in GaAs substrates with plasmonic gratings on the surface and standard THz photoconductive antenna [70].

vantage of this plasmonic grating realization is that only half of nonequilibrium electrons and holes reach the electrodes within subpicosecond time. This limits the effectiveness of such structures to 50 % [69].

In order to maintain the operation of the hybrid THz-optical photoconductive antenna without reducing its effectiveness, midway between the anode and the cathode grounding electrode is placed. This electrode is usually embedded into the semiconductor substrate and during a cycle of photoinduced charge carriers generation collects those electrons and holes that reach the electrodes, preventing their slow accumulation in the substrate. In the absence of a grounding electrode, these unwanted carriers recombine
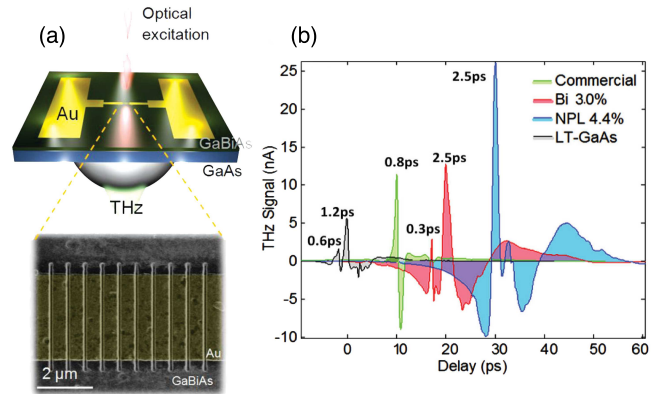
grating is low if compared to other methods, due to the large capacitance [180].

Figure 16 depicts another possible implementation of plasmonic nanorod gratings embedded in dipole photoconductive THz antenna. Instead of comb-like plasmonic grating structures described above, the ends of plasmonic nanorods in this configuration are connected together, which significantly shortens the path of the charge carriers to the electrodes. Moreover, this design allows reducing the capacitive reactance of the THz antenna that improves its emitting ability and increases the antenna gain coefficient. A disad-

Figure 15 (a) The geometry and SEM image of the THz dipole antenna with the unincorporated plasmonic grating. (b) THz signals of commercial THz antenna (green curve), dipole antenna with the GaAsBi semiconductor substrate (red curve), dipole antenna with the LT-GaAs substrate (black curve), and hybrid THz-optical antenna with the nanoplasmonic grating (blue curve).
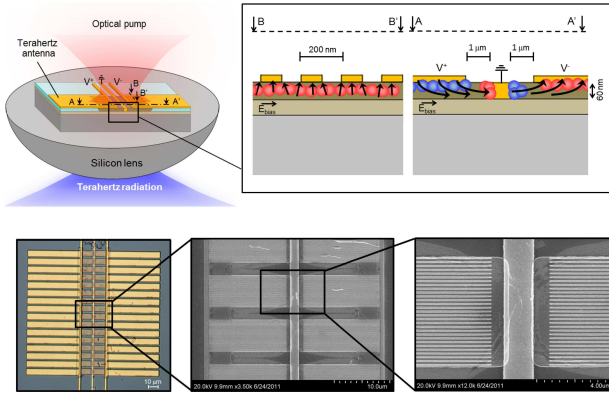
Figure 16 Structural diagram of the THz photoconductive antenna with embedded plasmonic nanorods and ground electrode, its principle of operation (top). Top view of an array of such antennas and their SEM image (bottom). [69]
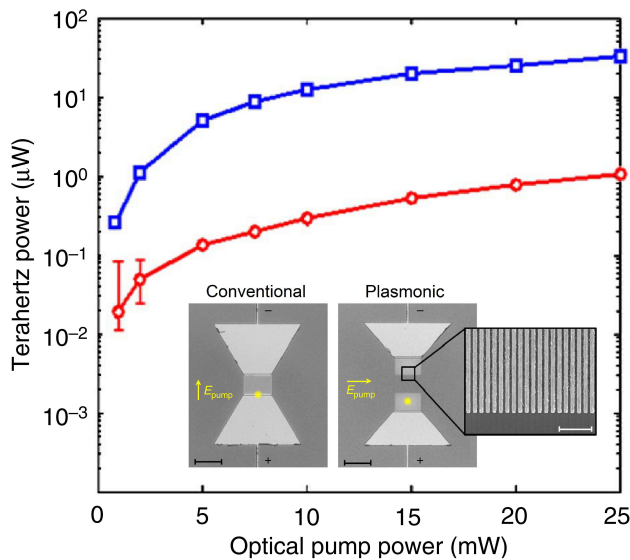

Figure 17 The THz output power vs. pump power for THz hybrid optical photoconductive antenna (blue) and a standard THz photoconductive antenna of the same geometry (red). [70]

with charges of opposite sign of the subsequent cycles of generation, thereby reducing the total number of particles that reach electrodes [69].

To manufacture such structures, the methods of electron-beam lithography, accompanied by the deposition of Au on LT-GaAs substrate are used. A dielectric layer covering NA reduces Fresnel reflection from its surface, thereby increasing the absorption coefficient of the optical pump into the substrate. Usually, 200 nm thick silica (SiO_2) is used for these purposes. This coating provides a 70% absorption of pump light into the semiconductor material.

Comparison of conventional THz photoconductive antennas and hybrid optical-to-THz antennas with integrated

plasmonic gratings reveals at least one order of magnitude superiority of the latter (Figure 17). Such a significant increase in the output power of THz radiation is achieved by reducing the path length of charge carriers to the electrodes, thus greatly increasing the photocurrent and decreasing the number of recombined electron-hole pairs.

An important role in THz hybrid optical photoconductive antennas is played by the thickness of the semiconductor substrate, since at a sufficiently large depths (over 100 nm) photoinduced charge carriers that do not participate in the effective generation of THz radiation start to accumulate. These electrons and holes rise from the depths of the substrate to the surface, where they recombine with other charges, thus significantly reducing the ratio of optical-terahertz conversion. To prevent negative effects caused by the non-equilibrium carriers accumulated in the lower layers of the substrate, its thickness should not exceed 100 nm. However, there is a workaround for this problem without reducing the thickness of semiconductor by using three-dimensional plasmonic gratings [90].

3.5. Three-dimensional plasmonic gratings

Plasmonic gratings described above are two-dimensional nanoscale structures on the semiconductor surface. They provide a high absorption of light quanta by a semiconductor material and significantly increase the concentration of photoinduced charge carriers near metal electrodes. However, the effectiveness of optical-terahertz conversion is still limited by the depth at which charge carriers are generated (~100 nm). To overcome this limitation, three-dimensional plasmonic gratings embedded in the semiconductor substrate are proposed. It has been shown, that such structures allow achieving 7.5% optical-to-THz conversion efficiency [90]. Figure 18 (a) shows a schematic of three-dimensional plasmonic gratings and distribution pattern of the absorbed optical radiation. Because of its complexity, the manufacturing of such antennas should be discussed in more detail. The process of three-dimensional plasmonic gratings fabrication starts with chemical vapor deposition of a 200 nm film of SiO_2 onto the surface of the semiconductor. Next, on the surface of the SiO_2 film, a nanoscale Nickel grid is applied by electron beam lithography. The grid serves as a template layer for etching of SiO_2. When using reactive ion etching with a source of inductively coupled plasma a SiO_2 grating is formed, which serves as a mask to create nano-walls made of semiconductor material. The plasmonic grating is obtained by deposition of gold on the sidewalls of the resulting semiconductor nanostructures. The height of the walls of the nanostructure determines the order of the modes excited in the resulting subwavelength waveguides. In such a structure waveguide TEM modes of 4th order can be excited by p-component of the fs-laser [185–187]. A SiO_2 mask is then removed by wet etching. Then to reduce the losses associated with reflection, the surface of the antenna is covered with a 200 nm layer of SiO_2. The resulting structure absorbs up to 70 percent of the incident laser radiation [187].
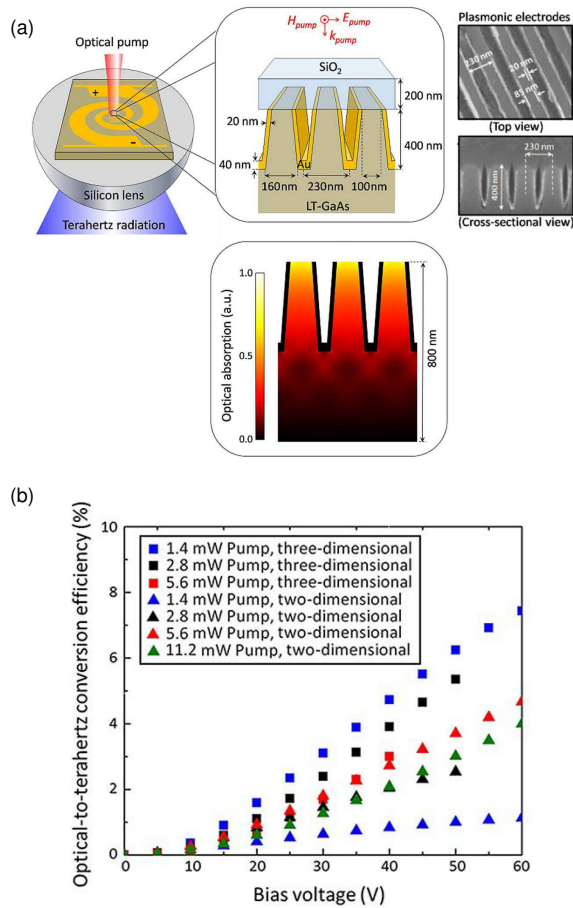
Figure 18 (a) Schematic representation of the logarithmic hybrid THz-optical and photoconductive antenna structures with integrated three-dimensional plasmonic structure, as well as its SEM picture. (b) The dependence of the optical-terahertz conversion on bias applied to antenna electrodes at different pump powers for THz photoconductive antennas with built-in two-dimensional and three-dimensional plasmonic gratings. [90]

Figure 18(b) demonstrates the advantages of three-dimensional gratings two-dimensional It is seen that three-dimensional plasmonic grating has a large coefficient of optical-to-THz conversion in comparison with the two-dimensional analogue. At the optical pump power of 1.4 mW, optical-to-THz conversion efficiency reaches 7.5%. Such efficiency increase is due to the fact that the three-dimensional plasmonic grating embedded into the surface layer of the semiconductor substrate, hence the contact surface of the grating with the semiconductor is much greater than that of the two-dimensional plasmonic gratings. This increases the concentration of the photoinduced charges near the metal electrodes, which are involved in the effective generation of THz radiation [90]. However, with increasing optical pump power, optical-to-THz conversion efficiency in three-dimensional structures decreases. This happens because a large number of separated electron-hole pairs gener-

ate a significant electric field with the direction opposite to the external field. The resulting field turns out to decrease, hence the efficiency of THz generation is reduced [71].

Thus, the THz photoconductive antennas with integrated three-dimensional plasmonic gratings provide greater efficiency of optical-to-THz conversion in comparison with two-dimensional plasmonic gratings. In the future, despite the complexity of fabrication technology, these three-dimensional nanoscale structures can replace two-dimensional in hybrid THz-optical photoconductive antennas.

4. Discussion and outlook

To summarize all results presented in the Review, we have gathered together studies on various approaches to the creation of hybrid photoconductive antennas for THz generation, in order to facilitate a direct comparison of the proposed methods (see Table 1). We conclude that the most high-performance hybrid THz photoconductive antennas are the ones based on three-dimensional plasmonic gratings with the maximum conversion efficiency of 7.5%, at the pump power of 1.4 mW. For comparison, hybrid THz photoconductive antennas based on two-dimensional plasmonic gratings have the maximum conversion efficiency of about 0.2% only, at a higher pump power 25 mW.

This Review has demonstrated obvious advantages of hybrid THz photoconductive antennas and photomixers over conventional ones, especially in their conversion efficiency at low pump powers. With the development of compact ultrafast fiber [189] and semiconductor [190, 191] lasers, followed by the use of new photoconductive materials suitable for the longer-wavelength, e.g. Yb-based lasers (1030 nm), Er-doped fiber lasers (1550 nm) or semiconductor quantum dot lasers (950–1300 nm) pumping, such as GaBiAs [192], InGaAs [193], and also containing ErAs [194], and InAs [66, 129, 195] quantum dots in GaAs substrates, these can lead to the creation of highly effective, miniature THz transmitters, working at room temperatures both in pulsed and CW regimes. Despite the complexity and high cost of hybrid electrodes fabrication, the total setup cost, that will exclude the extremely expensive titanium-sapphire laser, should significantly decrease.

Moreover, despite a number of plasmonic NAs' advantages associated with their small size and strong electric field localization, such NAs have large dissipative losses resulting in their low efficiency. To overcome such limitations, a new type of *nanoantennas based on dielectric nanoparticles* (e.g. silicon) with a high index dielectric constant has been recently proposed [196–201]. Such NAs could be very promising for hybrid THz-optical photoconductive antennas. Namely, they also have an ability to strong electric (and magnetic) local field enhancement [202–205]. Moreover, they have a much higher damage threshold due to low dissipative losses. The typical values of damage threshold for metallic nanostructures are: gold nanorods ($\sim$70 GW/cm^2 or $\sim$10 mJ/cm^2 at 130 fs [206]), gold G-shaped nanostructure ($\sim$ 100 GW/cm^2

Method of Plasmon Resonance Obtaining	Regime	Fabrication Complexity	Generation Enhancement Factor	Spectral range, THz	Maximum Conversion Efficiency	At Pump Power	# Ref.
Silver Nanoparticles	Pulse	Relatively Low	2x	0.1–1.1	–	50 mW	[165]
AuGe Nanoparticles	Pulse	Relatively Low	4x	0.1–1.5	–	–	[168]
Hexagonal Nanoantennas	Pulse	High	20x	0.1–2.4	–	2 mW	[74]
Interdigitated metallic dipole nanoantenna (six-nanofinger)	CW	Relatively Low	–	0.1–1.1	0.0002%	26 mW	[172]
Interdigitated metallic dipole nanoantenna (five-nanofinger)	CW	Relatively Low	–	0.1–1.1	0.0006%	50 mW	[188]
Interdigitated metallic dipole nanoantenna (eight-nanofinger)	CW	Relatively Low	–	0.1–1.1	0.007%	90 mW	[147]
Rectangular metal dipole nanoantennas	CW	High	4x	0.1–1.1	0.0005%	55 mW	[174]
Bow-tie metallic dipole nanoantennas	CW	High	7x	0.1–1.1	0.0008%	55 mW	[174]
Unincorporated plasmonic gratings	Pulse	High	4x	0.1–2.1	–	17 mW	[180]
Plasmonic gratings for impulse THz generation	Pulse	High	35x–50x	0.1–1.5	0.2%	25 mW	[70]
Plasmonic gratings for CW-THz generation	Pulse	High	20x	0.2–2.5	0.03%	50 mW	[86]
Plasmonic gratings with grounding electrode	Pulse	High	50x	0.1–1.5	0.005%	85 mW	[69]
3D plasmonic gratings	Pulse	Extremely High	1500x	0.1–3.0	7.5%	1.4 mW	[90]

Table 1 Comparison of the proposed fabrication methods of hybrid photoconductive antennas for efficient THz generation.

or $\sim$3 mJ/cm^2 at 30 fs [207]), and gold nanocylinders ($\sim$200 GW/cm^2 or $\sim$20 mJ/cm^2 at 100 fs [208]). According to the known data from literature, low-loss silicon nanoparticles have significantly higher damage threshold: $\sim$400 GW/cm^2 or $\sim$100 mJ/cm^2 at 250 fs [209]; and $\sim$1000 GW/cm^2 or $\sim$100 mJ/cm^2 at 100 fs [198]. Such considerable difference in damage thresholds for plasmonic (e.g. gold) and all-dielectric (e.g. silicon) materials originates from the difference in their melting temperatures (T$_m$(Au)=1337 K and T$_m$(Si)=1687 K) and enthalpies of fusion (H(Au)=12.5 kJ/mol and H(Si)=50.2 kJ/mol). In accordance with these basic parameters, silicon has much higher damage threshold than gold. Therefore, the all-dielectric NAs allow for applying of very high laser intensities which is promising for an effective THz generation.

Thus, despite a large number of research works in this area and very encouraging results, consensus about the advantage of a particular structure as the absorption enhancer of the pump radiation, and the magnifier of effective generation area in a semiconductor is not formed yet. This is a very young research area where more studies and experiments are needed, aimed primarily at the optimisation of the proposed methods and quest for new types of NAs. In addition, the search for more simple solutions to the problem of transfer of optical radiation into the largest possible nonequilibrium carrier pairs number in a semiconductor, increasing the speed of their movement through the creation of more intense local electric and magnetic fields and reduction of their lifetime by reducing their free path lengths is also needed.

5. Conclusion

In this Review, an approach to solving the problem of low energy conversion in THz photoconductive antennas and photomixers is extensively studied. The reviewed solution comprises the use of optical nanoantennas for enhancing the efficiency of pump laser radiation absorption in the antenna gap, reducing the lifetime of photoexcited carriers and improving antenna thermal efficiency. Within the Review, the general principles of photonic THz generation in semiconductor converters pumped with fs-optical pulses and double-wavelength CW laser radiation are described, followed by the particular focus of this work the description of the hybrid THz-optical photoconductive antennas and

their general principles of operation. Antennas are systematized by the principle of their operation and compared by their efficiency and performance. In particular, the results in this promising field obtained by researchers of hybrid THz-optical photoconductive antennas can be attributed to plasmon monopoles, metal dipole NAs, and 2D/3D plasmon gratings.

Acknowledgments

References

[1] D. G. Martin Van ExterCh Fattinger., Optics Letters **14**, 1128–1130 (1989).

[2] B. Ferguson and X. C. Zhang, Nat. Mater. **1**(1), 26–33 (2002).

[3] P. H. Siegel, IEEE Transactions on microwave theory and techniques **50**, 910–928 (2002).

[4] C. A. Schmuttenmaer, Chem. Rev. **104**(4), 1759–1780 (2004).

[5] M. Tonouchi, Nature Photonics **1**, 97–105 (2007).

[6] P. U. Jepsen, D. G. Cooke, and M. Koch, Laser & Photonics Reviews **5**(1), 124–166 (2011).

[7] M. F. Pereira, Optical and Quantum Electronics **46**(4), 491–493 (2014).

[8] X. T. Xie, B. F. Zhu, and R. B. Liu, New Journal of Physics **15**(10), 105015 (2013).

[9] A. W. Wharmby and R. L. Bagley, International Journal of Engineering Science **93**, 1–12 (2015).

[10] L. Ozyuzer, A. E. Koshelev, C. Kurter, N. Gopalsami, Q. Li, M. Tachiki, K. Kadowaki, T. Yamamoto, H. Minami, H. Yamaguchi, T. Tachiki, K. E. Gray, W. K. Kwok, and U. Welp, Science **318**(5854), 1291–1293 (2007).

[11] U. Welp, K. Kadowaki, and R. Kleiner, Nature Photonics **7**(9), 702–710 (2013).

[12] T. Kashiwagi, M. Tsujimoto, T. Yamamoto, H. Minami, K. Yamaki, K. Delfanazari, K. Deguchi, N. Orita, T. Koike, R. Nakayama, T. Kitamura, M. Sawamura, S. Hagino, K. Ishida, K. Ivanovic, H. Asai, M. Tachiki, R. A. Klemm, and K. Kadowaki, Japanese Journal of Applied Physics **51**(1R), 010113 (2011).

[13] J. A. Zeitler, P. F. Taday, D. A. Newnham, M. Pepper, K. C. Gordon, and T. Rades, J. Pharm. Pharmacol. **59**(2), 209–223 (2007).

[14] Y. S. Jin, G. J. Kim, and S. G. Jeon, Journal of the Korean Physical Society **49**, 513–517 (2006).

[15] T. Globus, D. Woolard, T. Khromova, T. Crowe, M. Bykhovskaia, B. Gelmont, J. Hesler, and A. Samuels, Journal of Biological Physics **29**(2-3), 89–100 (2003).

[16] P. D. Cunningham, N. N. Valdes, F. A. Vallejo, L. M. Hayden, B. Polishak, X. H. Zhou, J. Luo, A. K. Y. Jen, J. C. Williams, and R. J. Twieg, Journal of Applied Physics **109**(4), 043505–043505 (2011).

[17] E. P. Parrott and J. A. Zeitler, Applied Spectroscopy **69**(1), 1–25 (2015).

[18] K. Niessen, M. Xu, E. Snell, and A. Markelz, Thz microscopy measurements on inhibitor dependence of protein intramolecular modes, in: Infrared, Millimeter, and Terahertz Waves, (2013).

[19] K. Niessen, M. Xu, E. Snell, V. Cody, J. Pace, M. Schmidt, and A. Markelz, Detection enhancement of protein structural vibrations: Measurements and calculations, in: APS Meeting Abstracts, (2015).

[20] R. J. Falconer and A. G. Markelz, Journal of Infrared, Millimeter, and Terahertz Waves **33**(10), 973–988 (2012).

[21] H. Murakami, Y. Toyota, T. Nishi, and S. Nashima, Chemical Physics Letters **519**, 105–109 (2012).

[22] J. F. Federici, B. Schulkin, F. Huang, D. Gary, R. Barat, F. Oliveira, and D. Zimdars, Semiconductor Science and Technology **20**, S266 (2005).

[23] J. F. Federici, B. Schulkin, F. Huang, D. Gary, R. Barat, F. Oliveira, and D. Zimdars, Semicond. Sci. Technol. **20**(7), S266–S280 (2005).

[24] C. Corsi and F. Sizov, THz and Security Applications: Detectors, Sources and Associated Electronics for THz Applications (Springer Netherlands, 2014).

[25] M. F. Pereira and O. Shulika, Terahertz and Mid Infrared Radiation: Detection of Explosives and CBRN (Using Terahertz) (Springer Netherlands, 2014).

[26] F. Xin, H. Su, and Y. Xiao, Terahertz imaging system for remote sensing and security applications, in: Antennas and Propagation (APCAP), (2014), pp. 1335–1338.

[27] M. Massaouti, C. Daskalaki, A. Gorodetsky, A. D. Koulouklidis, and S. Tzortzakis, Appl. Spectrosc.(11), 1264–1269.

[28] X. Wu, B. Quan, X. Pan, X. Xu, X. Lu, C. Gu, and L. Wang, Biosensors and Bioelectronics **42**, 626–631 (2012).

[29] H. R. Park, K. J. Ahn, S. Han, Y. M. Bahk, N. Park, and D. S. Kim, Nano Lett. **13**, 1782–1786 (2013).

[30] S. J. Park, J. T. Hong, S. J. Choi, H. S. Kim, W. K. Park, S. T. Han, J. Y. Park, S. Lee, D. S. Kim, and Y. H. Ahn, Scientific Reports **4**, 4988 (2014).

[31] L. Xie, W. Gao, J. Shu, Y. Ying, and J. Kono, Scientific Reports **5**, 8671 (2015).

[32] M. Zhang and J. T. Yeow, IEEE Nanotechnology Magazine **10**, 30–38 (2016).

[33] T. S. Bui, T. D. Dao, L. H. Dang, L. D. Vu, A. Ohi, T. Nabatame, Y. Lee, T. Nagao, and C. V. Hoang, Scientific Reports **6**, 32123 (2016).

[34] A. G. Davies, E. H. Linfield, and M. B. Johnston, Phys. Med. Biol. **47**(21), 3679–3689 (2002).

[35] P. H. Siegel, Microwave Symposium Digest, 2004 IEEE MTT-S International **3**, 1575–1578 (2004).

[36] M. Kawase, T. Saito, M. Ogama, H. Uejima, Y. Hatsuda, S. Kawanishi, Y. Hirotani, M. Myotoku, K. Ikeda, H. Konishi, I. Iga, J. Yamakawa, S. Nishizawa, K. Yamamoto, and M. Tani, Analytical Sciences **27**(2), 209 (2011).

[37] C. Yu, S. Fan, Y. Sun, and E. Pickwell-MacPherson, Quantitative Imaging in Medicine and Surgery **2**(1), 33 (2012).

[38] P. C. Ashworth, E. Pickwell-MacPherson, E. Provenzano, S. E. Pinder, A. D. Purushotham, M. Pepper, and V. P. Wallace, Opt. Express **17**(15), 12444–12454 (2009).

[39] V. P. Wallace, A. J. Fitzgerald, E. Pickwell, R. J. Pye, P. F. Taday, N. Flanagan, and T. Ha, Appl. Spectrosc. **60**(10), 1127–1133 (2006).

[40] K. Shiraga, Y. Ogawa, T. Suzuki, N. Kondo, A. Irisawa, and M. Imamura, J. Infrared, Millimeter, Terahertz Waves **35**(5), 493–502 (2014).

[41] L. Rong, T. Latychevskaia, C. Chen, D. Wang, Z. Yu, X. Zhou, Z. Li, H. Huang, Y. Wang, and Z. Zhou, Sci. Rep. **5**, 8445 (2015).

[42] K. Coppin, J. Geach, I. Smail, L. Dunne, A. Edge, R. Ivison, S. Maddox, R. Auld, M. Baes, S. Buttiglione et al., Monthly Notices of the Royal Astronomical Society **416**(1), 680–688 (2011).

[43] F. Wyrowski, R. Güsten, K. Menten, H. Wiesemeyer, and B. Klein, Astronomy & Astrophysics **542**, L15 (2012).

[44] U. U. Graf, C. E. Honingh, K. Jacobs, and J. Stutzki, Journal of Infrared, Millimeter, and Terahertz Waves **36**(10), 896–921 (2015).

[45] A. V. Smirnov, A. M. Baryshev, S. V. Pilipenko, N. V. Myshonkova, V. B. Bulanov, M. Y. Arkhipov, I. S. Vinogradov, S. F. Likhachev, and N. S. Kardashev, Space mission millimetron for terahertz astronomy, in: Space Telescopes and Instrumentation 2012: Optical, Infrared, and Millimeter Wave, (2012).

[46] H. Maezawa, IEICE Transactions on Electronics **98**(3), 196–206 (2015).

[47] A. Rogalski and F. Sizov, Opto-Electronics Review **19**(3), 346–404 (2011).

[48] I. F. Akyildiz, J. M. Jornet, and C. Han, Phys. Commun. **12**, 16–32 (2014).

[49] T. Kürner and S. Priebe, J. Infrared, Millimeter, Terahertz Waves **35**(1), 53–62 (2014).

[50] J. Federici and L. Moeller, Journal of Applied Physics **107**(11), 111101 (2010).

[51] F. Hu and S. Lucyszyn, Noise analysis for multi-channel thz torchthermal infrared wireless communications systems, in: Microwave Conference (APMC), 2014 Asia-Pacific, (2014).

[52] S. Koenig, D. Lopez-Diaz, J. Antes, F. Boes, R. Henneberger, A. Leuther, A. Tessmann, R. Schmogrow, D. Hillerkuss, R. Palmer et al., Nature Photonics **7**(12), 977–981 (2013).

[53] C. L. Pan and J. W. Shi, 3 ultrawide-band sub-thz photonic wireless links, in: Microwave Photonics, (CRC Press, 2013), p. 97.

[54] Y. Karisan and K. Sertel, Wideband impedance-matched integrated transceivers for future thz-band wireless networks, in: Radio Science Meeting (USNC-URSI NRSM), 2013 US National Committee of URSI National, (2013), pp. 1–1.

[55] C. Wang, B. Lu, C. Lin, Q. Chen, L. Miao, X. Deng, and J. Zhang, Terahertz Science and Technology, IEEE Transactions on **4**(1), 75–85 (2014).

[56] J. O. Richardson, D. J. Wales, S. C. Althorpe, R. P. McLaughlin, M. R. Viant, O. Shih, and R. J. Saykally, The Journal of Physical Chemistry A **117**(32), 6960–6966 (2013).

[57] J. Xu, K. W. Plaxco, and S. J. Allen, Journal of chemical physics **124**(3), 36101 (2006).

[58] G. Siles, J. M. Riera, P. Garcia del Pino et al., Antennas and Propagation Magazine, IEEE **57**(1), 48–61 (2015).

[59] S. U. Hwu, K. DeSilva, and C. Jih, Terahertz (thz) wireless systems for space applications, in: Sensors Applications Symposium (SAS), 2013 IEEE, (2013), pp. 171–175.

[60] G. Ducournau, P. Szriftgiser, A. Beck, D. Bacquet, F. Pavanello, E. Peytavit, M. Zaknoune, T. Akalin, and J. F. Lampin, Terahertz Science and Technology, IEEE Transactions on **4**(3), 328–337 (2014).

[61] A. J. Seeds, H. Shams, M. J. Fice, and C. C. Renaud, Journal of Lightwave Technology **33**(3), 579–587 (2015).

[62] K. Vodopyanov, Laser Photonics Rev. **2**, 11–25 (2008).

[63] D. Saeedkia and S. Safavi-Naeini, J. Light. Technol. **26**(15), 2409–2423 (2008).

[64] T. Otsuji, T. Watanabe, S. Boubanga Tombet, A. Satou et al., Terahertz Science and Technology, IEEE Transactions on **3**(1), 63–71 (2013).

[65] I. Wilke, P. S. Dutta, and E. Slobodtchikov, Thz radiation emission from inpas and gainas crystals, in: Infrared, Millimeter, and Terahertz waves (IRMMW-THz), 2014 39th International Conference on, (2014), p. 1.

[66] R. R. Leyman, A. Gorodetsky, N. Bazieva, G. Molis, A. Krotkus, E. Clarke, and E. U. Rafailov, Laser Photon. Rev. **10**(5), 772–779 (2016).

[67] M. B. Johnston, Journal of Infrared, Millimeter, and Terahertz Waves **33**(4), 391–392 (2012).

[68] M. Tani, K. Yamamoto, E. S. Estacio, C. T. Que, H. Nakajima, M. Hibi, F. Miyamaru, S. Nishizawa, and M. Hangyo, Journal of Infrared, Millimeter, and Terahertz Waves **33**(4), 393–404 (2012).

[69] C. W. Berry and M. Jarrahi, New Journal of Physics **14**, 105029 (2012).

[70] C. Berry, N. Wang, M. Hashemi, M. Unlu, and M. Jarrahi, Nature Communications **4**, 1622 (2013).

[71] G. C. Loata, M. D. Thomson, T. Löffler, and H. G. Roskos, Applied Physics Letters **91**(23), 232506 (2007).

[72] T. Hattori, K. Egawa, S. i. Ookuma, and T. Itatani, Japanese journal of applied physics **45**(4L), L422 (2006).

[73] Z. Piao, M. Tani, and K. Sakai, Japanese Journal of Applied Physics **39**(1R), 96 (2000).

[74] A. Jooshesh, L. Smith, M. Masnadi-Shirazi, V. Bahrami-Yekta, T. Tiedje, T. E. Darcie, and R. Gordon, Optics express **22**(23), 27992–28001 (2014).

[75] K. B. Crozier, A. Sundaramurthy, G. S. Kino, and C. F. Quate, J. Appl. Phys. **94**, 4632 (2003).

[76] P. Biagioni, J. S. Huang, and B. Hecht, Rep. Prog. Phys. **75**, 24402 (2012).

[77] A. E. Krasnok, I. S. Maksymov, A. I. Denisyuk, P. A. Belov, A. E. Miroshnichenko, C. R. Simovski, and Y. S. Kivshar, Physics-Uspekhi **56**(6), 539 (2013).

[78] P. Bharadwaj, B. Deutsch, and L. Novotny, Advances in Optics and Photonics **1**, 438–483 (2009).

[79] X. Ni, N. K. Emani, A. V. Kildishev, A. Boltasseva, and V. M. Shalaev, Science **335**(6067), 427–427 (2012).

[80] A. E. Miroshnichenko, I. S. Maksymov, A. R. Davoyan, C. Simovski, P. Belov, and Y. S. Kivshar, Physica Status Solidi (RRL)-Rapid Research Letters **5**(9), 347–349 (2011).

[81] S. G. Park, K. H. Jin, M. Yi, J. C. Ye, J. Ahn, and K. H. Jeong, ACS nano **6**(3), 2026–2031 (2012).

[82] S. K. Patel and C. Argyropoulos, EPJ Appl. Metamat. **2**, 4 (2015).

[83] L. Novotny and N. van Hulst, Nature Photonics **5**, 83–90 (2011).

[84] A. E. Krasnok, A. P. Slobozhanyuk, C. R. Simovski, S. A. Tretyakov, A. N. Poddubny, A. E. Miroshnichenko, Y. S. Kivshar, and P. A. Belov, Scientific Reports **5**, 12956 (2015).

[85] M. Jarrahi, IEEE Trans. Terahertz Sci. Technol. **5**, 391–397 (2015).

[86] C. W. Berry, M. R. Hashemi, S. Preu, H. Lu, A. C. Gossard, and M. Jarrahi, Optics Letters **39**, 4522–4524 (2014).

[87] C. Berry, M. Hashemi, and M. Jarrahi, Journal of Infrared, Millimeter, and Terahertz Waves **33**(4), 393–404 (2013).

[88] C. W. Berry, M. R. Hashemi, and M. Jarrahi, Applied Physics Letters **104**(8), 081122 (2014).

[89] C. W. Berry, M. R. Hashemi, S. Preu, H. Lu, A. C. Gossard, and M. Jarrahi, Applied Physics Letters **105**(1), 011121 (2014).

[90] S. H. Yang, M. R. Hashemi, C. W. Berry, and M. Jarrahi, Terahertz Science and Technology, IEEE Transactions on **4**(5), 575–581 (2014).

[91] O. Mitrofanov, I. Brener, T. S. Luk, and J. L. Reno, ACS Photonics **2**(12), 1763–1768 (2015).

[92] L. Ju, B. Geng, J. Horng, C. Girit, M. Martin, Z. Hao, H. a. Bechtel, X. Liang, A. Zettl, Y. R. Shen, and F. Wang, Nat. Nanotechnol. **6**(10), 630–634 (2011).

[93] M. Shalaby, H. Merbold, M. Peccianti, L. Razzari, G. Sharma, T. Ozaki, R. Morandotti, T. Feurer, A. Weber, L. Heyderman, B. Patterson, and H. Sigg, Appl. Phys. Lett. **99**(4), 041110 (2011).

[94] M. Shalaby, J. Fabiańska, M. Peccianti, Y. Ozturk, F. Vidal, H. Sigg, R. Morandotti, and T. Feurer, Appl. Phys. Lett. **104**(17), 171115 (2014).

[95] L. Razzari, A. Toma, M. Shalaby, M. Clerici, R. P. Zaccaria, C. Liberale, S. Marras, I. a. I. Al-Naib, G. Das, F. De Angelis, M. Peccianti, A. Falqui, T. Ozaki, R. Morandotti, and E. Di Fabrizio, Opt. Express **19**(27), 26088 (2011).

[96] L. Razzari, A. Toma, M. Clerici, M. Shalaby, G. Das, C. Liberale, M. Chirumamilla, R. P. Zaccaria, F. Angelis, M. Peccianti, R. Morandotti, and E. Fabrizio, Plasmonics **8**(1), 133–138 (2012).

[97] C. Feuillet-Palma, Y. Todorov, A. Vasanelli, and C. Sirtori, Scientific Reports **3**, 1361 (2013).

[98] A. Toma, S. Tuccio, M. Prato, F. De Donato, A. Perucchi, P. Di Pietro, S. Marras, C. Liberale, R. Proietti Zaccaria, F. De Angelis, L. Manna, S. Lupi, E. Di Fabrizio, and L. Razzari, Nano Lett. **15**(1), 386–391 (2015).

[99] M. G. Krishna, S. D. Kshirsagar, and S. P. Tewari, Terahertz Emitters, Detectors and Sensors: Current Status and Future Prospects (INTECH Open Access Publisher, 2012).

[100] S. Winnerl, Journal of Infrared, Millimeter, and Terahertz Waves **33**(4), 431–454 (2012).

[101] K. Reimann, Reports Prog. Phys. **70**(10), 1597–1632 (2007).

[102] V. Apostolopoulos and M. Barnes, Journal of Physics D: Applied Physics **47**(37), 374002 (2014).

[103] M. B. Johnston, D. M. Whittaker, A. Corchia, A. G. Davies, and E. H. Linfield, Phys. Rev. B **65**, 165301 (2002).

[104] J. A. Fülöp, L. Pálfalvi, M. C. Hoffmann, and J. Hebling, Opt. Express **19**, 15090–15097 (2011).

[105] K. Ravi, W. R. Huang, S. Carbajo, E. A. Nanni, D. N. Schimpf, E. P. Ippen, and F. X. Kärtner, Optics express **23**(4), 5253–5276 (2015).

[106] E. Abraham, M. Cornet, A. O. Hamouda, J. Degert, and E. Freysz, Terahertz-field-induced second harmonic generation through pockels effect in gallium phosphide crystal, in: CLEO: QELS_Fundamental Science, (2014).

[107] K. Y. Kim, a. J. Taylor, J. H. Glownia, and G. Rodriguez, Nat. Photonics **2**(10), 605–609 (2008).

[108] A. Gorodetsky, A. D. Koulouklidis, M. Massaouti, and S. Tzortzakis, Phys. Rev. A - At. Mol. Opt. Phys. **89**(3), 1–6 (2014).

[109] P. Maine, D. Strickland, P. Bado, M. Pessot, and G. Mourou, IEEE J. Quantum Electron. **24**(2), 398–403 (1988).

[110] M. W. McCutcheon, D. E. Chang, Y. Zhang, M. D. Lukin, and M. Loncar, Opt. Express **17**(22), 9 (2009).

[111] C. J. Docherty and M. B. Johnston, J. Infrared, Millimeter, Terahertz Waves **33**(8), 797–815 (2012).

[112] L. Luo, I. Chatzakis, J. Wang, F. B. P. Niesler, M. Wegener, T. Koschny, and C. M. Soukoulis, Nat. Commun. **5**, 3055 (2014).

[113] D. K. Polyushkin, I. Marton, P. Racz, P. Dombi, E. Hendry, and W. L. Barnes, Phys. Rev. B **89**, 125426 (2014).

[114] A. Atrashchenko, A. Arlauskas, R. Adomavicius, A. Korotchenkov, V. P. Ulin, P. Belov, A. Krotkus, and V. P. Evtikhiev, Appl. Phys. Lett. **105**, 191905 (2014).

[115] L. Zhang, F. Buccheri, C. Zhang, and X. C. Zhang, Appl. Phys. Lett. **107**, 071107 (2015).

[116] T. Seifert, S. Jaiswal, U. Martens, J. Hannegan, L. Braun, P. Maldonado, F. Freimuth, A. Kronenberg, J. Henrizi, I. Radu, E. Beaurepaire, Y. Mokrousov, P. M. Oppeneer, M. Jourdan, G. Jakob, D. Turchinovich, L. M. Hayden, M. Wolf, M. Münzenberg, M. Kläui, and T. Kampfrath, Nat. Photonics **10**(7), 483–488 (2016).

[117] K. Kato, K. Takano, Y. Tadokoro, and M. Nakajima, Optics Letters **41**, 2125–2128 (2016).

[118] T. Matsui, S. Tomita, M. Asai, Y. Tadokoro, K. Takano, M. Nakajima, M. Hangyo, and H. Yanagi, Applied Physics A **122**, 157 (2016).

[119] Y. M. Bahk, G. Ramakrishnan, J. Choi, H. Song, G. Choi, Y. H. Kim, K. J. Ahn, D. S. Kim, and P. C. M. Planken, ACS Nano **8**, 9089–9096 (2014).

[120] P. A. Obraztsov, N. Kanda, K. Konishi, M. Kuwata-Gonokami, S. V. Garnov, A. N. Obraztsov, and Y. P. Svirko, Phys. Rev. B **90**, 241416(R) (2014).

[121] O. V. Kibis, M. R. da Costa, and M. E. Portnoi, Nano Lett. **7**, 3414–3417 (2007).

[122] L. V. Titova, C. L. Pint, Q. Zhang, R. H. Hauge, J. Kono, and F. A. Hegmann, Nano Lett. **15**, 3267–3272 (2015).

[123] L. G. Zhu, B. Kubera, K. F. Mak, and J. Shan, Scientific Reports **5**, 10308 (2014).

[124] B. S. Williams, Nat. Photonics **1**(9), 517–525 (2007).

[125] A. Valavanis, J. Zhu, J. Freeman, L. Li, L. Chen, A. Davies, E. Linfield, and P. Dean, Electron. Lett. **50**(4), 309–311 (2014).

[126] F. Wang, K. Maussang, S. Moumdji, R. Colombelli, J. R. Freeman, I. Kundu, L. Li, E. H. Linfield, A. G. Davies, J. Mangeney, J. Tignon, and S. S. Dhillon, Optica **2**(11), 944 (2015).

[127] Q. Lu, D. Wu, S. Sengupta, S. Slivken, and M. Razeghi, Sci. Rep. **6**, 23595 (2016).

[128] S. Slivken and M. Razeghi, Proc. of SPIE **9755**, 97550C (2016).

[129] A. Gorodetsky, N. Bazieva, and E. U. Rafailov, Quantum-dot based ultrafast photoconductive antennae for efficient thz radiation, in: SPIE Proc., (2016), p. 97370C.

[130] H. Sherry, R. Al Hadi, J. Grzyb, E. Öjefors, A. Cathelin, A. Kaiser, and U. R. Pfeiffer, Lens-integrated thz imaging arrays in 65nm cmos technologies, in: Radio Frequency Integrated Circuits Symposium (RFIC), 2011 IEEE, (2011), pp. 1–4.

[131] J. Van Rudd and D. M. Mittleman, JOSA B **19**(2), 319–329 (2002).

[132] D. Grischkowsky, S. Keiding, M. van Exter, and C. Fattinger, J. Opt. Soc. Am. B **7**(10), 2006–2015 (1990).

[133] I. S. Gregory, C. Baker, W. R. Tribe, I. V. Bradley, M. J. Evans, E. H. Linfield, G. Davies, and M. Missous, Quantum Electronics, IEEE Journal of **41**(5), 717–728 (2005).

[134] V. L. Malevich, Tech. Phys. Lett. **29**(3), 240–242 (2003).

[135] M. M. Nazarov, A. P. Shkurinov, A. A. Angeluts, and D. A. Sapozhnikov, Radiophys. Quantum Electron. **52**(8), 536–545 (2010).

[136] X. C. Zhang, Y. Jin, T. Hewitt, T. Sangsiri, L. Kingsley, and M. Weiner, Applied Physics Letters **62**, 2003–2005 (1993).

[137] V. Bespalov, V. Krylov, S. Putilin, and D. Staselko, Optics and Spectroscopy **93**(1), 148–152 (2002).

[138] X. C. Zhang and D. H. Auston, J. Appl. Phys. **71**(1), 326 (1992).

[139] D. H. Auston, K. P. Cheung, and P. R. Smith, Appl. Phys. Lett. **45**(3), 284–286 (1984).

[140] Q. Chang, D. Yang, and L. Wang, Broadband thz generation from photoconductive antenna, in: Progress in electromagnetics research symposium, (2005), pp. 331–335.

[141] C. W. Berry and M. Jarrahi, Journal of Infrared, Millimeter, and Terahertz Waves **33**(12), 1182–1189 (2012).

[142] S. E. Ralph and D. Grischkowsky, Applied Physics Letters **59**(16), 1972–1974 (1991).

[143] E. R. Brown, F. W. Smith, and K. A. McIntosh, J. Appl. Phys. **73**(3), 1480–1484 (1993).

[144] K. McIntosh, E. Brown, K. Nichols, O. McMahon, W. DiNatale, and T. Lyszczarz, Applied Physics Letters **67**(26), 3844–3846 (1995).

[145] Y. S. Lee, Principles of Terahertz Science and Technology (Springer US, Boston, MA, 2009).

[146] C. A. Balanis, Antenna Theory: Analysis and Design, 3rd editio edition (Wiley-Blackwell, 2005).

[147] S. M. Duffy, S. Verghese, K. McIntosh, A. Jackson, A. Gossard, and S. Matsuura, Microwave Theory and Techniques, IEEE Transactions on **49**(6), 1032–1038 (2001).

[148] E. Brown, International Journal of High Speed Electronics and Systems **13**(02), 497–545 (2003).

[149] R. Mendis, C. Sydlo, J. Sigmund, M. Feiginov, P. Meissner, and H. Hartnagel, Antennas and Wireless Propagation Letters, IEEE **4**, 85–88 (2005).

[150] M. Jarrahi, High-efficiency terahertz sources based on plasmonic contact electrodes, in: 2015 IEEE MTT-S Int. Microw. Symp., (IEEE, may 2015), pp. 1–4.

[151] P. Maraghechi and A. Elezzabi, Optics Express **18**(26), 27336–27345 (2010).

[152] G. M. Rebeiz, Proceedings of the IEEE **80**(11), 1748–1770 (1992).

[153] E. Brown, A. Lee, B. Navi, and J. Bjarnason, Microwave and optical technology letters **48**(3), 524–529 (2006).

[154] S. Matsuura, M. Tani, and K. Sakai, Applied Physics Letters **70**(5), 559–561 (1997).

[155] M. Tani, S. Matsuura, K. Sakai, and S. i. Nakashima, Applied optics **36**(30), 7853–7859 (1997).

[156] K. Ezdi, M. Islam, Y. Reddy, C. Jördens, A. Enders, and M. Koch, A numerical study of photoconductive dipole antennas: the real emission frequency and an improved antenna design, in: Photonics Europe, (2006), p. 61940G.

[157] S. Verghese, K. McIntosh, and E. Brown, Microwave Theory and Techniques, IEEE Transactions on **45**(8), 1301–1309 (1997).

[158] I. Gregory, W. Tribe, B. Cole, M. Evans, E. Linfield, A. Davies, and M. Missous, Applied Physics Letters **85**(9), 1622–1624 (2004).

[159] T. K. Nguyen, H. Han, and I. Park, Journal of Infrared, Millimeter, and Terahertz Waves **32**(6), 763–777 (2011).

[160] S. Lal, S. Link, and N. J. Halas, Nature Photonics **1**, 641–648 (2007).

[161] V. Giannini, A. I. Fernandez-Dominguez, S. C. Heck, and S. A. Maier, Chem. Rev. **111**, 3888–3912 (2011).

[162] M. L. Brongersma and P. G. Kik, Surface plasmon nanophotonics (Springer, 2007).

[163] J. Shah, Hot Carriers in Semiconductor Nanostructures (Elsevier Inc., 1992).

[164] S. V. Makarov, V. A. Milichko, I. S. Mukhin, I. I. Shishkin, D. A. Zuev, A. M. Mozharov, A. E. Krasnok, and P. A. Belov, Laser and Photonics Reviews **10**, 91–99 (2016).

[165] S. G. Park, Y. Choi, Y. J. Oh, and K. H. Jeong, Optics express **20**(23), 25530–25535 (2012).

[166] Y. J. Oh and K. H. Jeong, Advanced Materials **24**(17), 2234–2237 (2012).

[167] K. W. Vogt and P. A. Kohl, Journal of Applied Physics **74**(10), 6448–6450 (1993).

[168] H. Surdi, A. Singh, and S. Prabhu, Enhancement of terahertz emission using auge nano-patterns, in: Proceedings of the 2013 COMSOL Conference in Bangalore, (2013).

[169] A. Singh, S. Pal, H. Surdi, S. Prabhu, V. Nanal, and R. Pillay, Applied Physics Letters **104**(6), 063501 (2014).

[170] T. A. Liu, M. Tani, M. Nakajima, M. Hangyo, and C. L. Pan, Applied physics letters **83**(7), 1322–1324 (2003).

[171] I. C. Mayorga, M. Mikulics, A. Schmitz, P. Van der Wal, R. Gusten, M. Marso, P. Kordos, and H. Luth, An optimization of terahertz local oscillators based on lt-gaas technology, in: SPIE Astronomical Telescopes+ Instrumentation, (2004), pp. 537–547.

[172] R. Mendis, C. Sydlo, J. Sigmund, M. Feiginov, P. Meissner, and H. L. Hartnagel, Solid-State Electronics **48**(10), 2041–2045 (2004).

[173] G. Seniutinas, G. Gervinskas, E. Constable, A. Krotkus, G. Molis, G. Valušis, R. Lewis, and S. Juodkazis, Thz photomixer with a 40nm-wide nanoelectrode gap on low-temperature grown gaas, in: SPIE Micro+ Nano Materials, Devices, and Applications, (2013), p. 892322.

[174] N. Khiabani, Y. Huang, L. E. Garcia-Munoz, Y. C. Shen, and A. Rivera-Lavado, Terahertz Science and Technology, IEEE Transactions on **4**(4), 501–508 (2014).

[175] M. D. Wissert, A. W. Schell, K. S. Ilin, M. Siegel, and H. J. Eisler, Nanotechnology **20**(42), 425203 (2009).

[176] E. Michael, B. Vowinkel, R. Schieder, M. Mikulics, M. Marso, and P. Kordoš, Applied physics letters **86**(11), 111120 (2005).

[177] Y. Hou, J. Liu, M. Buchanan, A. S. Thorpe, P. Poole, H. Liu, K. Wu, S. Roorda, and X. Zhang, Nano-Micro Letters **4**(1), 10–13 (2012).

[178] H. Tanoto, J. Teng, Q. Wu, M. Sun, Z. Chen, S. Maier, B. Wang, C. Chum, G. Si, A. Danner et al., Scientific reports **3**, 2824 (2013).

[179] M. Seo, H. Park, S. Koo, D. Park, J. Kang, O. Suwal, S. Choi, P. Planken, G. Park, N. Park et al., Nature Photonics **3**(3), 152–156 (2009).

[180] B. Heshmat, M. Masnadi-Shirazi, R. B. Lewis, J. Zhang, T. Tiedje, R. Gordon, and T. E. Darcie, Adv. Opt. Mater. **1**(10), 714–719 (2013).

[181] B. Heshmat, H. Pahlevaninezhad, Y. Pang, M. Masnadi-Shirazi, R. Burton Lewis, T. Tiedje, R. Gordon, and T. E. Darcie, Nano Lett. **12**(12), 6255–9 (2012).

[182] A. Jooshesh, V. Bahrami-Yekta, J. Zhang, T. Tiedje, T. E. Darcie, and R. Gordon, Nano Lett. **15**(12), 8306–8310 (2015).

[183] C. W. Berry and M. Jarrahi, Plasmonically-enhanced localization of light into photoconductive antennas, in: Conference on Lasers and Electro-Optics, (2010), p. CFI2.

[184] A. Krotkus, A. Arlauskas, and R. Adomaviius, Semiconductor investigation by terahertz radiation pulses (2012), pp. 84960V–84960V–10.

[185] P. B. Catrysse, G. Veronis, H. Shin, J. T. Shen, and S. Fan, Applied Physics Letters **88**(3), 031101 (2006).

[186] B. Y. Hsieh and M. Jarrahi, Journal of Applied Physics **109**(8), 084326 (2011).

[187] S. H. Yang and M. Jarrahi, Optics letters **38**(18), 3677–3679 (2013).

[188] I. S. Gregory, C. Baker, W. Tribe, M. Evans, H. E. Beere, E. H. Linfield, A. Davies, and M. Missous, Applied physics letters **83**(20), 4199–4201 (2003).

[189] M. E. Fermann and I. Hartl, Nat. Photonics **7**(11), 868–874 (2013).

[190] E. U. Rafailov, M. A. Cataluna, and W. Sibbett, Nat. Photonics **1**(7), 395–401 (2007).

[191] M. A. Gaafar, A. Rahimi-Iman, K. A. Fedorova, W. Stolz, E. U. Rafailov, and M. Koch, Adv. Opt. Photonics **8**(3), 370 (2016).

[192] K. Bertulis, A. Krotkus, G. Aleksejenko, V. Pacebutas, R. Adomavicius, G. Molis, and S. Marcinkevicius, Appl. Phys. Lett. **88**(20), 201112 (2006).

[193] M. Suzuki and M. Tonouchi, Appl. Phys. Lett. **86**(5), 051104 (2005).

[194] A. Krotkus and J. L. Coutaz, Semicond. Sci. Technol. **20**(7), S142–S150 (2005).

[195] E. Estacio, M. H. Pham, S. Takatori, M. Cadatal-Raduban, T. Nakazato, T. Shimizu, N. Sarukura, A. Somintac, M. Defensor, F. C. B. Awitan, R. B. Jaculbia, A. Salvador, and A. Garcia, Appl. Phys. Lett. **94**, 232104 (2009).

[196] A. E. Krasnok, D. Filonov, C. Simovski, Y. Kivshar, and P. Belov, Applied Physics Letters **104**, 133502 (2014).

[197] A. B. Evlyukhin, S. M. Novikov, U. Zywietz, R. L. Eriksen, C. Reinhardt, S. I. Bozhevolnyi, and B. N. Chichkov, Nano Letters **12**(7), 3749–3755 (2012).

[198] S. Makarov, S. I. Kudryashov, I. Mukhin, A. Mozharov, V. Milichko, A. Krasnok, and P. A. Belov, Nano Letters **15**(9), 6187–6192 (2015).

[199] A. Krasnok, S. Makarov, M. Petrov, R. Savelev, P. Belov, and Y. Kivshar, SPIE Opt. and Optoelectr. **9502**, 950203–950203 (2015).

[200] A. E. Krasnok, A. E. Miroshnichenko, P. A. Belov, and Y. S. Kivshar, Opt. Express **20**, 20599–20604 (2012).

[201] A. E. Krasnok, C. R. Simovski, P. A. Belov, and Y. S. Kivshar, Nanoscale **6**, 7354–7361 (2014).

[202] R. M. Bakker, D. Permyakov, Y. F. Yu, D. Markovich, R. Paniagua-Dominguez, L. Gonzaga, A. Samusev, Y. S. Kivshar, B. Luk'yanchuk, and A. I. Kuznetsov, Nano Lett. **15**, 2137–2142 (2015).

[203] R. Savelev, S. Makarov, A. Krasnok, and P. Belov, Optics and Spectroscopy (2015).

[204] P. A. Dmitriev, D. G. Baranov, V. A. Milichko, S. V. Makarov, I. S. Mukhin, A. K. Samusev, A. E. Krasnok, P. A. Belov, and Y. S. Kivshar, Nanoscale **8**, 9721–9726 (2016).

[205] S. V. Makarov, A. Tsypkin, T. Voytova, V. Milichko, I. Mukhin, A. Yulin, S. Putilin, M. Baranov, A. Krasnok, I. A. Morozov, and P. Belov, Nanoscale **DOI: 10.1039/C6NR04860A** (2016).

[206] G. A. Wurtz, R. Pollard, W. Hendren, G. P. Wiederrecht, D. J. Gosztola, V. A. Podolskiy, and A. V. Zayats, Nature Nanotechnology **6**(2), 107–111 (2011).

[207] V. K. Valev, D. Denkova, X. Zheng, A. I. Kuznetsov, C. Reinhardt, B. N. Chichkov, G. Tsutsumanova, E. J. Osley, V. Petkov, B. D. Clercq, A. V. Silhanek, Y. Jeyaram, V. Volskiy, P. A. Warburton, G. A. E. Vandenbosch, S. Russev, O. A. Aktsipetrov, M. Ameloot, V. V. Moshchalkov, and T. Verbiest, Advanced Materials **24**, OP29–OP35 (2012).

[208] D. A. Zuev, S. V. Makarov, V. A. Milichko, S. V. Starikov, I. S. Mukhin, I. A. Morozov, I. I. Shishkin, A. E. Krasnok, and P. A. Belov, Adv. Mater. **28**, 3087–3093 (2016).

[209] Y. Yang, W. Wang, A. Boulesbaa, I. I. Kravchenko, D. P. Briggs, A. Puretzky, D. Geohegan, and J. Valentine, Nano Lett. **15**(11), 7388–7393 (2015).